UNIVERSITY OF TWENTE.

Analysing the dependencies of cross-shore evolution of near-bed orbital velocity on physical parameters

Yulai Wang

MSc. Thesis

Water Engineering & Management

University of Twente

The Netherlands

September 2016

Supervision committee:

Head supervisor: Dr. Ir. Jan S. Ribberink

University of Twente

Daily supervisor: Dr. Ir. Angels Fernandez-Mora

University of Twente

External supervisor: Dr. Ir. Jebbe van der Werf

University of Twente, Deltare

Summary

The wave motion is tightly connected with morphological development, since the near-bed velocities provide the driving force for sediment transport. Waves propagate to shoreline with transformation of their shapes to skewed (shorter and higher crests and longer and shallower troughs) and asymmetric (a steep front face and a gentle rear face), which results in net cross-shore sediment transport. Thus a proper expression of near-bed orbital velocity under skewed and asymmetric waves is vital to accurate predictions on morphological evolution. In practice, parameterisations are applied to predict the evolution to avoid the problem caused by computationally expensive simulation. However, the performances of most parametrisations are unsatisfactory regarding the results of computed skewness and asymmetry of near-bed orbital velocity, including the commonly-used model of Ruessink *et al.* (2012).

The research objective is to determine wave shoaling and breaking effects on the near-bed orbital velocity skewness and asymmetry in order to improve the Ruessink's parameterisation. The research is done based on the wave data simulated by the CFD model waves2Foam. To confirm the correctness of model results, the model is tested using detailed elevation, velocity, and turbulence data measured in the CIEM flume, Barcelona in the framework of SINBAD research project.

Model validation is done regarding hydrodynamics variables surface elevation, near-bed orbital velocity, time-averaged turbulence, and relative variables such as the Ursell number, the near-bed skewness and asymmetry, and etc.. Broadly, the prediction capacity of waves2Foam is acceptable enough for this research. Therefore waves2Foam is considered reliable, and hence its simulations can be applied in dependencies analysis as important data source.

Six cases are simulated for dependencies research. In specific, two regular wave conditions (wave height 0.5m and wave height 0.8m with the same wave period 4.0s) on three linear sloping bed (1/15, 1/20, and 1/25). To achieve the research objective, physical parameters are considered as wave height, wavelength, surf similarity parameter, the Ursell number, wave energy dissipation, roller dissipation, dissipation by bed friction, and near-turbulence. The near-bed skewness and asymmetry depend on these physical parameters to different extent respectively. It is found that the dependencies on Ursell number and roller dissipation are potential to be further parameterise.

The dependencies on the Ursell number under regular waves on linear beds are different with the field data of irregular waves on barred beach. Thus, Ruessink' parameterisation can be adjusted accordingly by using Ursell number under different conditions. Moreover, the roller dissipation is in large potential for further parameterisation, as it can be simplified by wave height and wave length under the condition of this research.

Contents

Chapter 1

Introduction

1.1 Research background

The orbital motion of the water particles of waves change from purely circular in the deep sea to increasingly elongated ellipse in shallow water. Consequently, the near-bed orbital motion is unavoidably influenced. Specifically, its oscillation over time is sinusoidal in the deep sea, while becomes irregular when waves gradually approach the coastline. The non-linearity can be categorised as skewness and asymmetry. A skewed wave has higher and shorter crest, and shallower and longer trough. Moreover, an asymmetric wave behaves as saw-tooth with steep front and gentle rear face. Figure 1.1 shows the pure skewed wave (panel A) and pure asymmetric wave (panel B) respectively.

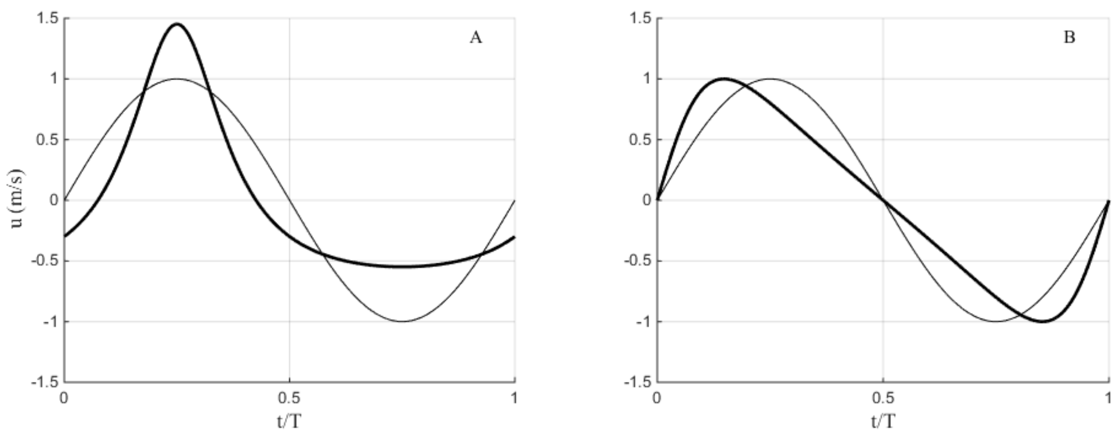

Figure 1.1 The comparisons of the near-bed orbital velocity between sinusoidal shape and, panel A pure skewed shape, and panel B pure asymmetric shape. The near-bed orbital velocity is calculated by the expression in Abreu *et al.* (2010).

According to Ruessink *et al.*, 2012, skewness and asymmetry are defined as Eqn. (1.1) and (1.2) respectively:

$$Sku = \frac{< {u_0}^3 >}{\delta_{u_0}^3} \tag{1.1}$$

$$Asu = \frac{< \Im {u_0}^3 >}{\delta_{u_0}^3} \tag{1.2}$$

where $\tilde{\imath}$ is the horizontal near-bed orbital velocity, $< >$ means phase average, δ is the standard deviation of u_0, and $\Im$ represents the Hilbert transform (Elgar, 1987).

Being an essential driving factor to morphological development, the motion of near-bed water particles is highly relevant to coastal and nearshore engineering. Also, it was proved that skewed and asymmetric wave results in onshore bar migration (Elgar *et al*., 2001, Ruessink *et al*., 2011). Therefore a proper expression of the cross-shore near-bed orbital motion is essential to morphodynamics prediction. Accurate prediction in terms of water surface and outer fluxes can be presented by advanced wave models, like Reynolds-Averaged Navier-Stokes models (e.g. Jacobsen *et al*., 2012), Boussinesq models (e.g. Kennedy *et al*., 2010), Large eddy simulation (e.g. Christensen and Rolf, 2001), and Direct numerical simulation (e.g. Kim *et al*.,). However, they are too computationally demanding to be used for mid- and long-term morphodynamics simulations. Therefore, some morphological models have implemented existing parameterization of near-bed orbital velocity which drives sediment transport. These parameterizations have been developed to predict the orbital velocity shape using relatively simple analytical expressions. Using water depth, (deep-water) wave height, wavelength, and bed slope, Isobe and Horikawa (1982) parameterized both skewned and asymmetric near-bed velocity for regular waves at normal incidence. Elfrink *et al*. (2006) derived a different piecewise function of near-bed velocity for irregular shoaling waves at normal incidence based on a large amount of field data. However, both functional forms of Isobe and Horikawa (1982) and Elfrink *et al*. (2006) are discontinuous regarding velocity and corresponding acceleration (Abreu *et al*. 2010; Malarkey and Davies 2012).

Based on the work of Drake and Calantoni. (2001), Abreu *et al*. (2010) derived a parameterization of near-bed velocity which calculates continuous regular time series which are approximation of Isobe and Horikawa (1982) and Elfrink *et al*. (2006). However, Abreu *et al*. (2010) work is cumbersome and requires solving cubic equations (Malarkey and Davies, 2012). Ruessink et al., (2012) characterised a simpler parameterization of skewness and asymmetry, which can be applied in the analytical expression of near-bottom velocity of Abreu et al., (2010) to simulate velocity time series.

Van den Broek (2015) used data from SINBAD fixed bed experiment (Van der A. *et al*. to be submitted) to test three parameterizations of Isobe and Horikawa (1982), Elfrink *et al*. (2006), Ruessink *et al*. (2012) (hereafter referred as Ruessink parameterization. Ruessink parameterisation better predicted in velocity peaks and troughs, and skewness than the other two methods. However, the deviations of Ruessink parameterisation predictions are still inaccurate regarding underestimation of skewness and asymmetry. An improved parameterisation is necessary for sand transport models when an accurate prediction is required, especially in the breaking zone (Van den Broek, 2015).

Two reasons could explain this mismatch between Ruessink's method and the experimental data. One is that Ruessink *et al*., (2012) calibrated their parameterisation with irregular waves from field observation, while Van den Broek (2015) used regular and unidirectional wave data in experiment. Consequently, "Ruessink parameterisation may underestimate skewness of orbital velocity in laboratory wave" (Ruessink *et al*., 2012), since irregular waves do not break intensively while regular waves do. The other is that the most vital input of Ruessink parameterisation is defined by the Ursell number which is calculated according to linear wave theory. However, wave shoaling and breaking are non-linear processes due to wave deformation, which may cause the mismatch of Ruessink parameterisation.

Although Ruessink parameterisation defects are noticeable, it has the large potential to be further improved because it is simply computed, is able to predict pronounced bar migration, and can be applied in Abreu's expression to generate continuous wave series. Besides the Ursell number, some other physical processes (introduced in the section 1.3 in this chapter) are hypothesized to relate the near-bed orbital velocity skewness and asymmetry. These physical processes, as well as the Ursell number, are going to be analysed in order to improve the prediction capacity of Ruessink parameterisation.

1.2 Research objective and questions

Based on the drawbacks of Ruessink parameterisation prediction, the research objective is:

To determine wave shoaling and breaking effects on the near-bed orbital velocity skewness and asymmetry in order to improve the parameterisation by Ruessink et al. (2012).

As parameterisation is derived from large amount of data, in this research model waves2Foam (described in the next section) is used as wave data generator. Simulated data is going to be studied in order to achieve the research objective. Therefore three research questions are formulated as:

1. How well can wave2Foam simulate near-bed orbital velocity under regular waves?

    1.1 What experimental data is available for model validation?

    1.2 Can waves2Foam satisfactory predict surface elevation, cross-shore elevation profiles, and the Ursell number?

    1.3 Can waves2Foam satisfactorily predict near-bed orbital velocity, cross-shore velocity profiles, skewness and asymmetry?

    1.4 Can wave2Foam satisfactorily predict vertical time-averaged turbulence?

2. How do wave shoaling and breaking affect the near-bed orbital velocity?

    2.1 Which physical parameters are associated to wave shoaling and breaking?

    2.2 Do the near-bed skewness and asymmetry depend on these physical parameters?

    2.3 How is these relations affected by bed slope and wave height?

3. How can the Ruessink parameterisation be improved?

    3.1 Which physical parameters associated wave shoaling and breaking are potential for parameterisations?

3.2 How can the effect of shoaling and breaking on near-bed orbital velocity be parameterised under the condition of regular waves on linear beds?

1.3 Research tools

1.3.1 waves2Foam

The computational fluid dynamics (CFD) model waves2Foam (Jacobsen *et al.* 2012) coupled with SediMorph (sediment transport model) is a wave generator which uses the Reynolds-Averaged Navier-Stokes equations coupled with a volume of fluid method to solve two-phase flow problems. For turbulence, modified *k-ε* and *k-ω* shear stress transport models (Brown *et al*. 2014, 2016) are embedded. In this research, the simulated turbulence data is based on *k-ε* model, because *k-ε* model is more reliable than the other according to a test (personal communication with Fernandez-Mora A., June, 2016). The high resolution is desired to simulate accurately wave motion, especially near-bed processes. Since the spatial domains for all runs are different, the grids are accordingly unlike (introduced in Chapter 2). The model outputs consist of velocity field (horizontal, vertical, and lateral), water-air interface coefficient, sediment concentration, turbulence, turbulence dissipation, eddy viscosity, and pressure. The outputs are stored in C++ ASCII files at each computational point per time step.

1.3.2 MATLAB

MATLAB is mainly used in this research in terms of:

1. selecting the required data from whole data set. The required data is introduced in Chapter 2, and the essential selecting methods are presented in Appendix B.
2. treating selected the selected data in needed formations for different usages. The method of data treatment is given in Appendix B.
3. computing required physical parameters based on the treated data for model validation and case studies respectively. The expressions of physical parameters are shown in Chapter 2.
4. for case studies , analysing the dependencies of near-bed skewness and asymmetry on physical parameters which is further fitted based on the method in the last section in Chapter 2.

1.4 Research approaches and outlines

Ruessink *et al.* (2012) derived the parameterisation with the data on barred beaches with water depth h between 0.25 and 11.2m, and irregular waves with significant wave height H_s between 0.05 and 3.99m, and period T between 3.1 and 13.9s. This research focuses on simpler cases, regular waves on linear beds, as the primary step to understand the dependencies of near-bed skewness and asymmetry on wave shoaling and breaking. The wave conditions are designed within the validity range of Ruessink's method as wave height H=0.5m and 0.8m with same period T=4.0s. Moreover the deep water depth is 2.55m. The wave conditions and deep water depth are designed referring to SINBAD mobile bed experiment in CIEM flume (introduced in Chapter 2). This research is a start of the analysis of the dependencies of near-bed skewness and asymmetry on other physical parameters. To simply the analysis, the linear sloping bed are considered. The bed slopes are chosen as 1/15, 1/20, and 1/25 to investigate the bed slope effects on the dependencies. Moreover, this research as the extend study regarding bed slopes of Ruessink' work, as Ruessink *et al.* (2012) suggested the bed slope gentler than 1/30.

For the research question "*1. How well can wave2Foam simulate near-bed orbital velocity under regular waves?*", the experimental data (SINBAD mobile bed project) for model validation, and the validation run of model are introduced in Chapter 2. Then Chapter 3 shows the results of model validation regarding surface elevation, near-bed orbital velocity and turbulence themselves, and other variables based them, e.g. cross-shore profile of surface elevation.

The research questions "*2. How do wave shoaling and breaking affect the near-bed orbital velocity?*" and "*3. How can the Ruessink parameterisation be improved?*" are tightly related, i.e., research question 3 is answered based on the findings in research question 2. Chapter 2 introduces the simulated physical parameters which are associated to wave shoaling and breaking. They are chosen from basic to complex as wave height, wave length, surf similarity, the Ursell number, energy dissipation (wave energy dissipation, roller dissipation, and dissipation due to bed friction), and near-bed turbulence. The dependencies of near-bed skewness and asymmetry on the Ursell number is confirmed by Ruessink *et al.* (2012) under irregular wave conditions on barred beaches, and is going to be analysed in this research for regular waves. Surf similarity is chosen for investigating slope effects. Furthermore, energy dissipation and near-bed turbulence are detailed physical processes, and are hypothesized to relate to near-bed skewness and asymmetry. Chapter 4 presents the dependencies analysis which is done by relating near-bed skewness and asymmetry as functions of physical processes. And the physical parameters- which are clearly related to relation to near-bed skewness and asymmetry are selected for further discussion in Chapter 5 where research question 3 is answered partly.

This thesis finally presents conclusions with answering the research questions and the recommendations for further research.

Chapter 2

Methodology

The research methodology is described in this chapter. Section 2.1 introduces the available experimental data (SINBAD mobile bed project) for model validation. Section 2.2 presents the model simulations for validation and designed cases respectively. Then the calculations of interesting physical parameters which are associated to wave shoaling and breaking are shown in Section 2.3, while the fitting techniques are briefly introduced in Section 2.4. The according data treatment, e.g. data selection, data averaging, is shown in Appendix B.

2.1 SINBAD mobile bed experiment

2.1.1 Experiment set-up

The experiment was done in the CIEM wave flume (at Universitat Politecnica de Catalunya in Barcelona) with a length of 100m, a width of 3m and 4.5m depth. Figure 2.1 shows the experimental set-up. The x-axis shows the cross-shore position in the flume where the paddle was located at x=0m. Z-axis indicates the positons upwards in the flume where the still water level (SWL) was set at z=0m. The foreslope was 1:10, and a breaker bar was located between 50m and 58m. After the breaker bar was an 18m long and 1.35m deep horizontal bed followed by a dissipative beach. Figure 2.1 bottom panel depicts the shoaling region (x<55.5m), breaking region (55.5<x<59.0m), and inner surf zone where roller develops (x>59.0m) (Van der Zanden *et al*. 2016). The breaking point was not fixed and slowly shifted onshore due to morphological evolution. The wave paddle was located at x=0m with 2.55m water depth. It generated regular waves with wave height H=0.85m and wave period T=4.0s. Firstly the initial bed developed for 105 minutes. Then the reference bed profile (Figure 2.1 upper panel) for measurement was made by levelling out cross-flume asymmetries and bed forms in the drained flume.

2.1.2 Measurements

The measurement lasted 12 experimental days and consisted of 6 15-minute runs per day. The data of the first 15-minute run is used for model validation in this research. Cross-shore measurement locations ranged from x=51.0m to x=63.0m with the spacing interval of 0.5m to 3.0m. Thus the measurements could record the waves from shoaling to bore developing.

Several instruments were installed at 12 locations in the measurement region (see Figure 2.1b) for different usages. Data from the following instruments is used in this research:

1. surface elevation: Pore Pressure Transducers (PPTs) that measured free surface elevation in 40Hz in the breaking zone. Note that surface elevation measured by Resistive Wave Gauges (RWGs) is not considered in this research, because the

wave splash-up affected the electronics of RWGs and reduced measured data quality (Van der Zanden *et al*. 2016).

2. near-bed velocities: Acoustic Doppler Velocimeters (ADVs) sampled the velocities in 100Hz at about 11cm, 41cm, and 85cm above the bed, respectively. The measured velocities are in three dimensions, horizontal, lateral, and vertical. ACVP measured only near-bed velocity at frequency of 70Hz. Since the near-bed velocity data from ACVP is similar to ADVs data concerning root mean square, maxima, minima, skewness and asymmetry (not shown in the thesis), it is not considered in model validation.
3. turbulence components: which were obtained from ADVs at 100Hz, in horizontal, lateral and vertical directions respectively. Turbulence measured by ACVP is not considered, because it was only recorded at near-bed layer, while the validation of turbulence should be done along the water column.

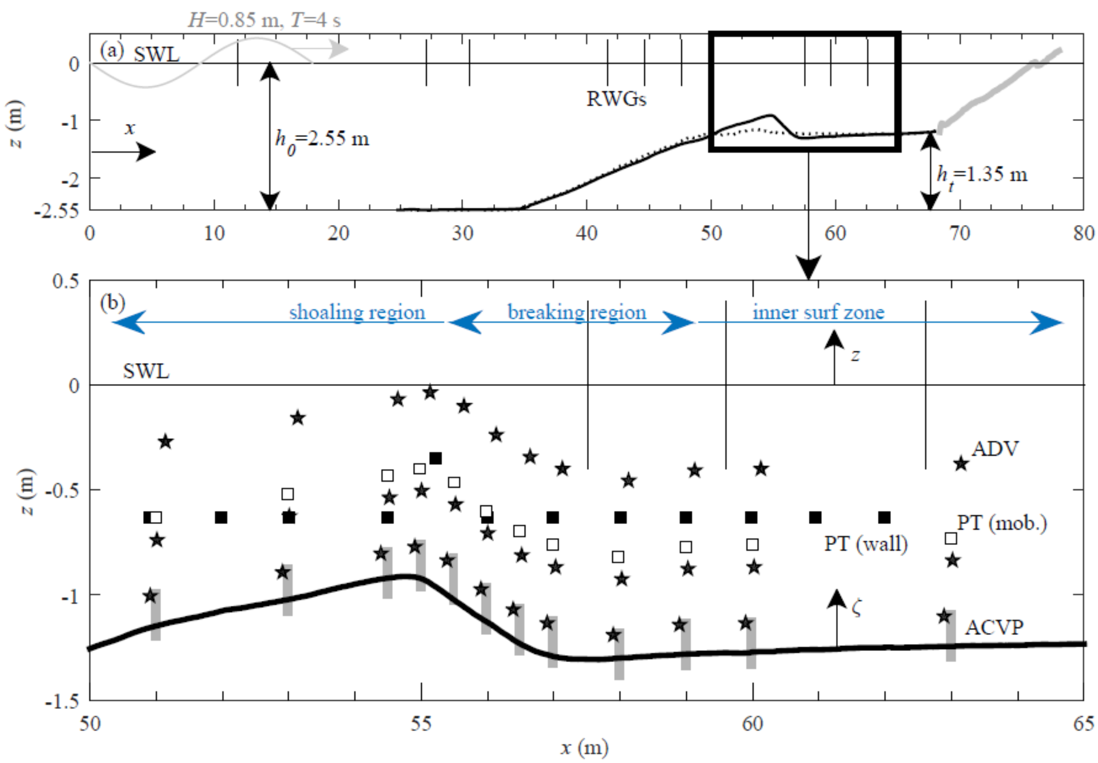

Figure 2.1"Bed profile and measuring locations. (a) General overview of wave flume, including initial horizontal test section (dotted line), reference bed profile (solid bold black line), fixed beach (solid gray line) and locations of resistive wave gauges (black vertical lines, not at full scale); (b) Close-up of test section, including reference bed profile and instrument positions: mobile-frame pressure transducer ('PT mob'.; white squares); wall-deployed PTs (black squares); mobile-frame ADVs (stars); and ACVP sampling profiles (gray rectangles)." (Source: Van der Zanden et al. 2016)

2 Model simulations

2.2.1 SINBAD simulation

To reproduce SINBAD mobile bed experiment, waves2Foam simulated the constantly incoming waves with the wave height of 0.85m and wave period of 4.0s. The total runtime of the simulation was 48.25s (due to model instability) with the time step of 0.05s, i.e., about 12 waves were simulated. The equilibrium will be discussed in Chapter 3.

The geometry was already set as the reference profile with the breaker bar. As can be seen from Figure 2.1a, the channel length was set to approximately 79m. The toe of the slope, breaker bar, and horizontal test zone had the same coordinates comparing with experimental set-up. The vertical domain was from -2.55m to 1.4m where 0m was SWL.

The height of grid gradually becomes finer from about 6.7cm at top to 0.1cm at bottom. And the length of grid is around 4.0cm near breaker bar. The computational points were built for SINBAD simulation as 81 by 1543 (z-direction by x-direction), i.e. 124983 computational points in total.

2.2.2 Designed cases

Ruessink *et al.* (2012) stressed that their parameterisation is suitable for irregular waves on bed with slopes (smaller than 1:30). To improve Ruessink parameterisation, it is necessary to study the wave motions under the conditions which are proposed as the limitation by Ruessink *et al.* (2012). Ruessink *et al*. (2012) measured waves with significant wave height H_s between 0.05 and 3.99m, T between 3.1 and 13.9s, and h between 0.25 and 11.2m. To ensure the chosen waves are within validity regime, and break within similar location on the same bed profile, two regular waves are designed based on AMORFO70 model (Fernandez-mora A. 2015). One with H=0.5m and T= 4.0s (hereafter referred as H05T4), and the other with H=0.8m and T= 4.0s (hereafter referred as H08T4). Three different slopes are chosen: 1:15 (SL15), 1:20 (SL20) and 1:25 (SL25). And all cases are referred as abbreviations hereafter, for example, H05T4-SL15 stands for the case that wave with 0.5m wave height and 4.0s period propagates on the linear bed with slope of 1:15. Table 2.1 illustrates the study area for all cases including shoaling zones, breaking zones, and inner surf zones. The breaker type is determined by breaking moment of simulated water surface (not shown in this thesis).

The contour maps of depth-averaged turbulence (Appendix A) are used as an auxiliary tool to find the splash point as the right boundary of breaking zone. Besides, the left boundary is determined according to Battjes and Jassen (1978) who describes that wave breaks at its maximum wave height (not shown in this research). The bed profiles for case studies can be seen in Figure 2.2.

Table 2.1 An overview of the locations of research area, and breaker type for each case.

	Slope					
	SL15		SL20		SL25	
	H05T4	H08T4	H05T4	H08T4	H05T4	H08T4
Shoaling	40m-54.5m	40m-54m	50m-64.5m	50m-64m	61m-76m	60m-75.5m
Breaking	54.5m-56.5m	54m-56m	64.5m-66.5m	64m-66m	76m-78m	75.5m-78m
Inner surf	56.5m-60m	56m-60m	66.5m-70m	66m-70m	78m-81m	78m-81m
Breaker	Plunging	Plunging	Plunging	Plunging	Plunging	Plunging

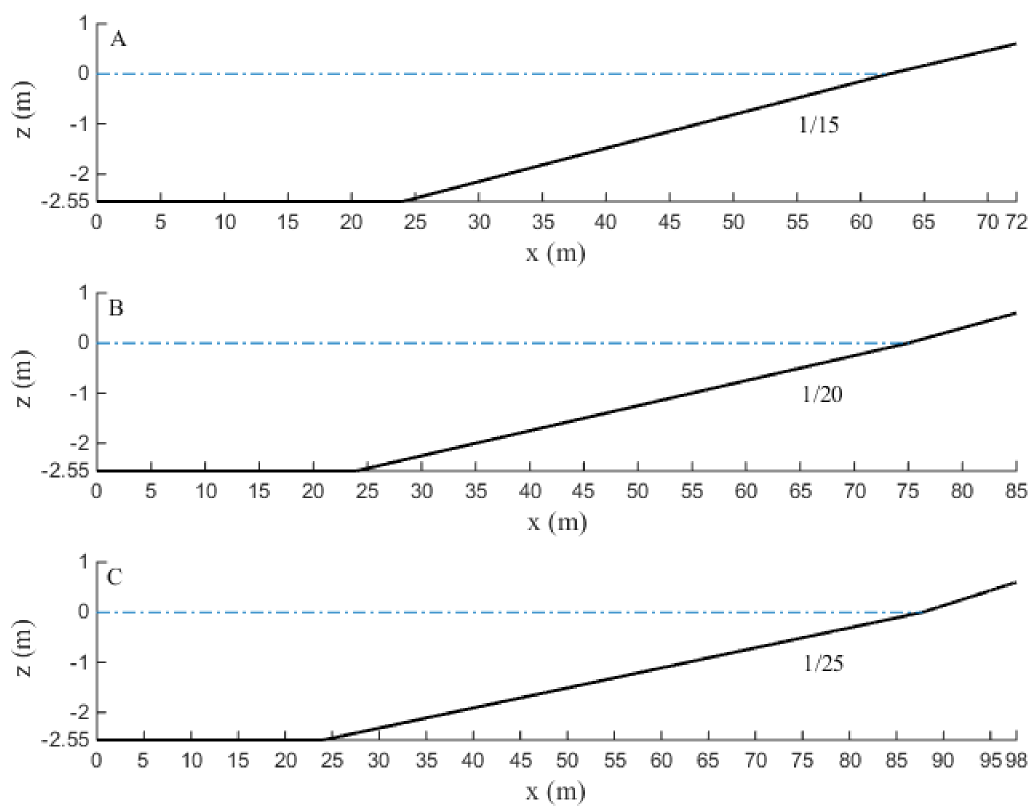

Figure 2.2 The designed linear sloping bed profiles (dark thick lines) with slope, panel A 1/15, panel B 1/20, and Panel C 1/25. The blue dashed lines are the still water level.

2.3 Physical parameters

2.4.1 Basic wave parameters

The wave height H and the wavelength L, the most fundamental parameters of waves, are considered to associate wave shoaling and breaking. According to the linear wave theory, wave height naturally increases with shoaling then decreases with breaking. Also, the wave height itself is a necessary input for other physical parameters such as the Ursell number, surf similarity parameter, wave energy dissipation, and dissipation due to bed friction. The wave height is calculated as

$$H = <\eta(t)>_{\max} - <\eta(t)>_{\min} \tag{2.1}$$

where $<\eta(t)>$ is the phase averaged surface elevation (phase averaging is given in Appendix B). Moreover, the wavelength gradually decreases with the wave propagating from shoaling zone to inner surf zone. The expression of wavelength is $L = 2\pi / k$, where k is the wave number solved from dispersion relation $\omega^2 = gk\tanh(kh)$ with local water depth h and angular frequency ω.

2.4.2 Ursell number

The Ursell number is validated to experimental one. And, it is studied for all case to compare regular waves with linear beds with field data of irregular waves on barred beach (Ruessink *et al.* 2012). The expression of the Ursell number is given by Doering and Bowen (1995) as

$$Ur = \frac{3}{8}\frac{Hk}{(kh)^3} \tag{2.2}$$

2.4.3 Surf similarity

Based on the deep water surf similarity given by Battjes (1974), local surf similarity parameter is computed as

$$\xi = \frac{i_b}{\sqrt{H/L}} \tag{2.3}$$

where i_b is the bed slope. The surf similarity contains bed slope, which is favourable for the analysis of the slope effects. Moreover, the wave steepness (H/L) is included in the expression, thus the surf similarity parameter is related to wave shoaling and breaking.

2.4.4 Energy dissipation

The energy dissipation consists of wave energy dissipation D_w which contains the wave height, dissipation due to bottom friction D_f which contains wave height and wave number (hence wavelength), and roller dissipation D_r, associated with turbulence, is an independent process from basic wave parameters. Hence, D_w and D_f are studied for investigated the dependencies of near-bed skewness and asymmetry on basic wave parameters with complex formations. While *D*r is studied for the effects of turbulence related term on near-bed skewness and asymmetry. The expression of these dissipations are given as follow:

Wave energy dissipation D_w

$$D_w = -\frac{\partial(cE_w)}{\partial x} \tag{2.4}$$

Where c is the wave celerity; and E_w is the wave energy according to Svendsen (1984)

$$E_w = \frac{1}{8}\rho g H^2 \tag{2.5}$$

where ρ is the density of sea water. Roller dissipation is written as

$$D_r = \rho \frac{\hat{\upsilon}(t)}{M} \tag{2.6}$$

where M is a constant input; and $\hat{\upsilon}(t)$ is the depth and time averaged eddy viscosity (averaging method is given in Appendix B). And, dissipation due to bottom friction is incorporated by Battjes and Jassen (1978) in the energy dissipation model. An approximation to it can be described as

$$D_f = \frac{f_w \rho}{\sqrt{\pi}} U_w^{\ 3} \tag{2.7}$$

where $f_w = \exp[5.2(\frac{U_w}{k_n})^{-0.19} - 6]$ is the friction factor; and U_w is the amplitude of near-bed orbital velocity

$$U_w = \frac{H\omega}{2} \frac{\cosh kz_0}{\sinh kh} \tag{2.8}$$

where z_0 is set to 0.1m above the bed; and k_n is Nikuradse's equivalent sand roughness.

2.4.5 Turbulence

The turbulence k (Note differentiate with the wave number) is the other independent process from wave height and wavelength. It is researched for the same purpose of *D*r. For all model simulations, turbulence is one of the outputs in time series. For model validation and case studies, it is treated to depth-averaged data for the determination of hydrodynamics for all simulations. Besides, it is treated to time-averaged data for model validation and dependencies analysis respectively.

2.4 Fitting methods

To fit the dependencies of near-bed skewness and asymmetry on physical parameters, the least square technique is mainly applied in this research. Since the theoritcal equations for least square, as well as the corresponding MATLAB codes are cumbersome, they are briefly introduced here. For linear or nearly linear dependencies, polynomial least square with 1 degree is used to find the best fits. For non-linear dependencies, the best fits are found according to one of polynomial least square with high degree, and exponential least square. All the resolved best fits are evaluated by the coefficient of determination R^2 which is computed as

$$R^2 = 1 - \frac{\sum_{i=1}^{N}(y - y_i)^2}{\sum_{i=1}^{N}(y - \overline{y})^2} \tag{2.9}$$

where y is the raw data; y_i is fitting results; N is the amount of pointwise dependencies; and the overbar in Eqn. (2.9) is the mean.

Chapter 3

Model validation

This chapter focuses on validation of model waves2Foam with SINBAD experimental data. Firstly, in Section 3.1, in order to obtain periodic wave data for model validation, the hydrodynamics equilibrium is determined for SINBAD simulation regarding surface elevation, near-bed orbital velocity and depth-averaged turbulence. Then, waves2Foam simulation is evaluated: in Section 3.2, surface elevation and corresponding cross-shore profiles and the Ursell number; in Section 3.3, near-bed orbital velocity and corresponding cross-shore profiles, skewness and asymmetry; and in Section 3.4, vertical profiles of time-averaged turbulence, and the cross-shore trend of time-averaged near-bed turbulence. Besides, Ruessink parameterisation is considered in the comparisons in Section 3.2 to test its perdition capacity under regular waves.

3.1 Hydrodynamics equilibrium

For all the model simulations, waves start to propagate from x=0m at t=0s. The system takes time to reach hydrodynamics equilibrium after which waves are more periodic and hence favourable to research. As the model became unstable and crashed, the SINBAD simulation stopped at runtime 48.20s which was about 12 wave periods. To determine the time point when hydrodynamics equilibrium is reached, three time-dependent variables - surface elevation, near-bottom velocity, and depth-averaged turbulence - are applied. As the turbulence validation is done at positions of ADVs along the water column, the equilibrium of turbulence should be considered wholly along water column. The depth-averaged turbulence is thus chosen instead of near-bed turbulence.

The oscillation of the water surface at the measurement locations are presented in Figure 3.1. It can be observed that the surface elevations are relatively smooth from 50.9m to 55.2m, and are increasingly discontinuous from 56.0m to 62.0m. The discontinuity of surface elevation after breaking point (55.5m) can be considered as the limitation of used tracking approach. As water and air interacts with each other intensively after breaking point, the use of constant α (0.8) cannot capture properly the water surface which is strongly affected by air bubbles. Nevertheless, discontinuous surface elevation series does not influence the analysis of equilibrium.

Focusing on the envelopes, it can be seen from 50.9m to 55.2m the peaks and troughs of surface elevation tend to be stable after the 6th wave period (24s runtime), despite there are slight changes. After 56.0m (from panel F to L), the changes of crests and troughs are still can be observed after the 6th wave period, while the change rate becomes relatively small after the 8th wave period (runtime 32s). Thus, in the studied region, the equilibrium of surface elevation is reached at the 8th wave period.

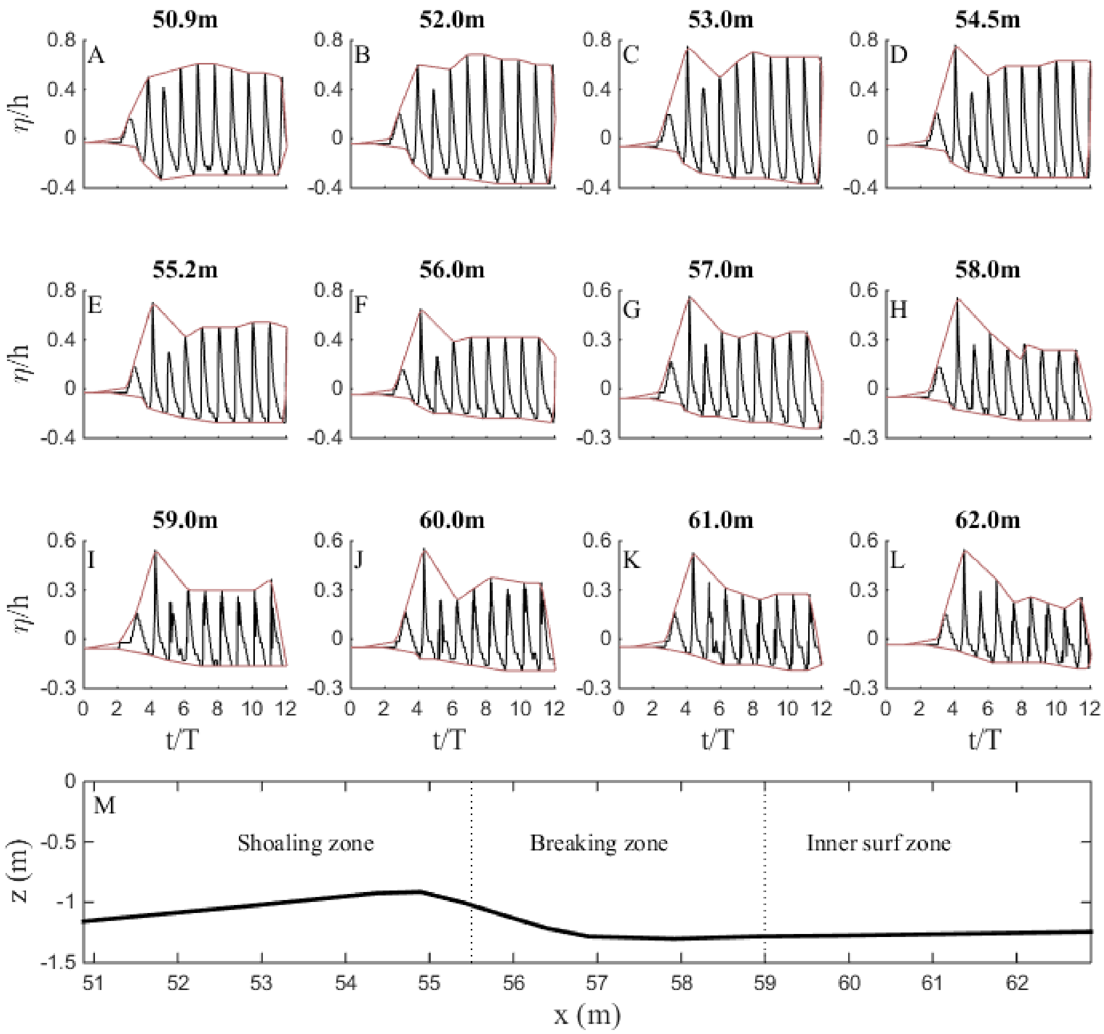

Figure 3.1 Dimensionless surface elevation as a function of time. The light red lines are the envelopes. Panels A to L are measurement locations in the cross-shore order. Panel M is the measurement area, the thick dark line is the bed profile; the dotted dark lines partition the study region as shoaling zone, breaking zone, and inner surf zone.

Figure 3.2 illustrates that the near-bed orbital velocities oscillate over time. It can be seen from the envelopes that both maxima and minima of velocities are nearly stable after the 8th wave period between 50.9m and 57.0m, although the velocity maxima at 55.4m and 55.9m tends to rise. The near-bed orbital velocities at the remaining measurement locations slightly vary after the 8th wave period. Especially, the velocity minima at 57.9m continuously decreases, and at 62.9m moderately both maxima and minima fluctuate in small range. However, it is acceptable to determine that the near-bed orbital velocity in equilibrium broadly after the 8th wave period.

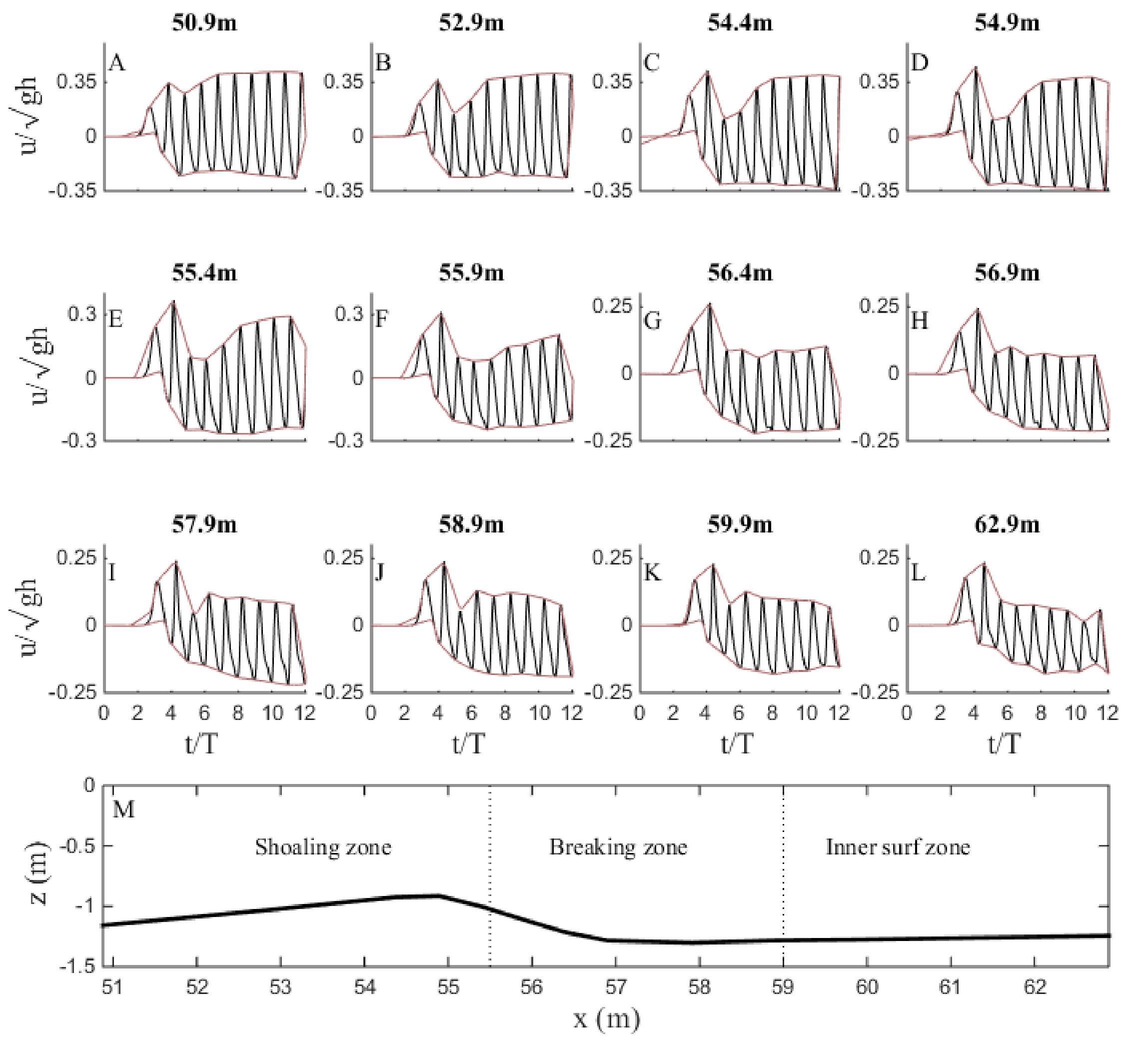

Figure 3.2 Dimensionless near-bed orbital velocity as a function of time. The light red lines are the envelopes. Panels A to L are measurement locations in the cross-shore order. Panel M is the measurement area, the thick dark line is the bed profile; the dotted dark lines partition the study region as shoaling zone, breaking zone, and inner surf zone.

Figure 3.2 shows the time-dependent depth-averaged turbulence at the measurement locations. According to the envelopes between 51.0m and 55.0m, it can be seen that the depth-average turbulence is stable after the 8th wave period. Namely, the depth-average turbulence in the shoaling zone is in equilibrium after then. When looking at breaking zone (from 55.5m to 59.0m) and inner surf zone (60.0m and 63.0m), the depth-averaged turbulence in does not reach the equilibrium until the end of simulation. It likely reaches equilibrium after the 12th wave period. One thing can be confirmed that the depth-averaged turbulence in study region takes longer to reach equilibrium than surface elevation and near-bed orbital velocity. To determine the equilibrium of depth-averaged turbulence, this research considers more weights on shoaling and breaking zones, because the processes in inner surf zone is more dynamic and difficult to be reach perfect equilibrium like the other zones. Therefore, the equilibrium time of depth-averaged turbulence (and the water system) is determined at the 8th wave period for model validation. Consequently, the time-averaged turbulence in breaking zone and inner surface zone is less accurate, and the quantitative validation is influenced. However, the qualitative validation is less affected, because it is done for testing that the at which ADV position the simulated turbulence is the most reliable.

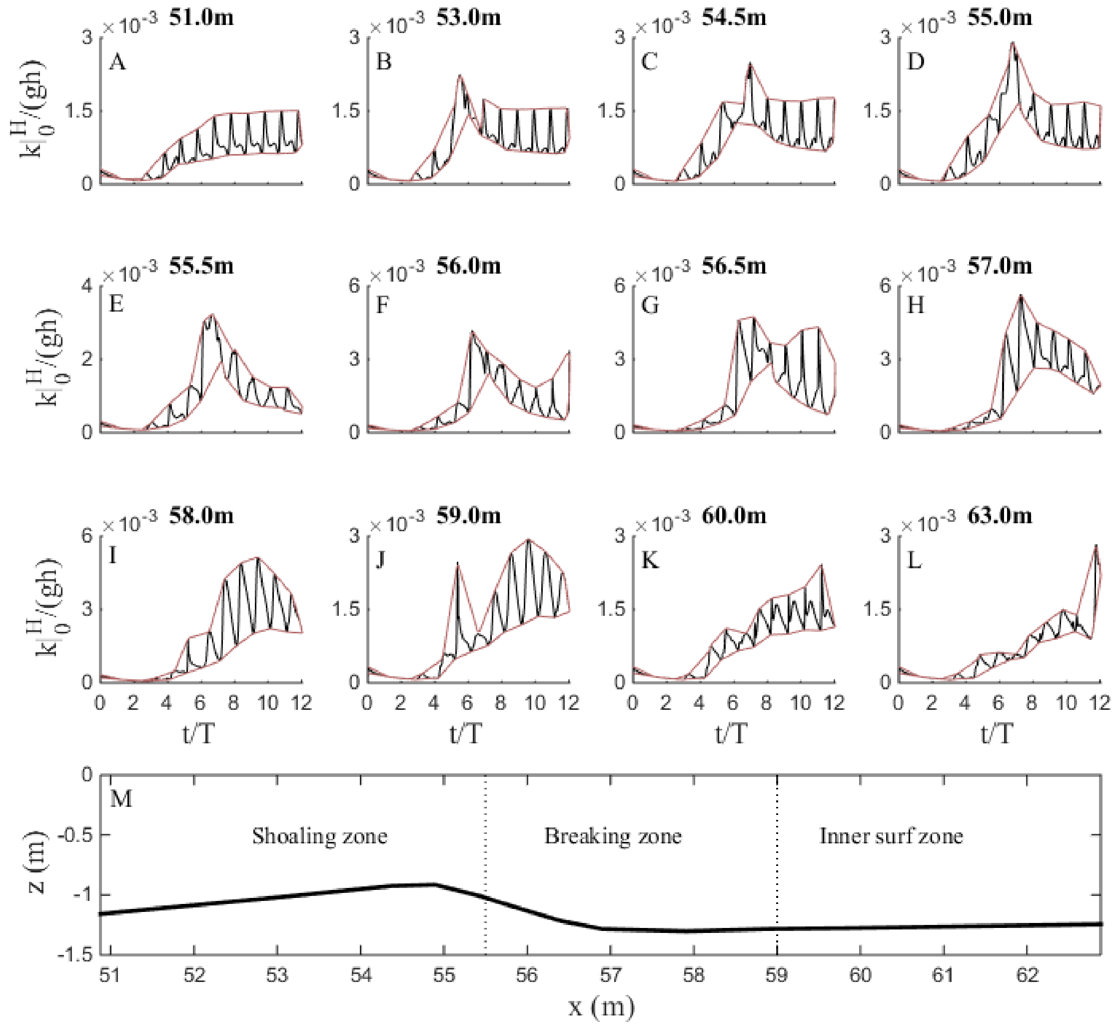

Figure 3.3 Dimensionless depth-averaged turbulence as a function of time. The light red lines are the envelopes. Panels A to L are measurement locations in the cross-shore order. Panel M is the measurement area, the thick dark line is the bed profile; the dotted dark lines partition the study region as shoaling zone, breaking zone, and inner surf zone.

3.2 Surface elevation

Figure 3.4 compares the phase-averaged surface elevation between wave2Foam and SINBAD data. Here the normalised root mean square error (NRMSE) is introduced to facilitate the comparisons between simulated data with different sacels. NRMSE is calculated as:

$$NRMSE = \frac{1}{y_{\max} - y_{\min}} \sqrt{\frac{1}{N} (x_i - y_i)^2} \tag{3.1}$$

where N is the amount of time step within one period; x represents dimensional simulated data; y represents the dimensional experimental data.

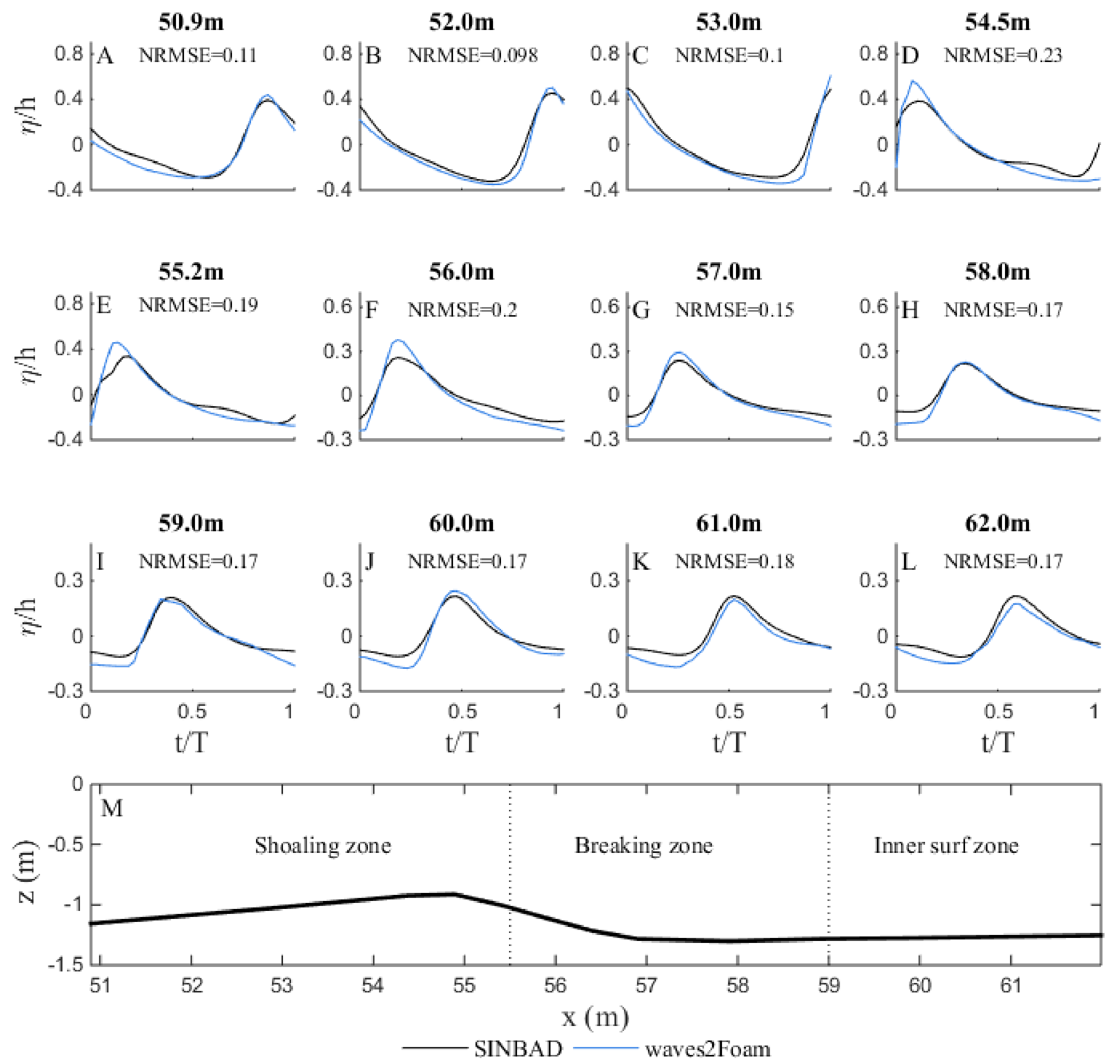

Figure 3.4 Comparing dimensionless phase-averaged surface elevation of waves2Fom with SINBAD data. Panels A to L indicate the locations of PPTs. The normalised root mean square error is represented by NRMSE. Panel M is the measurement area, the thick dark line is the bed profile; the dotted dark lines partition the study region as shoaling zone, breaking zone, and inner surf zone.

It can be seen that the simulated phase-averaged elevations broadly match the experimental data. Moreover, the wave shape transformation is satisfactorily captured by waves2Foam. The most observable mismatches with average NRMSE of 0.21 are from 54.5m to 56.0m, where the elevation crests are overestimated. This could be partly caused by surface tracking process. The phase-averaged simulated surface elevations at the rest locations are satisfactorily simulated with average NRMSE of approximately 0.15.

Based on phase-averaged surface elevation, the further comparisons are presented in Figure 3.5. It can be seen in panel A that waves2Foam satisfactorily predicted the mean elevation. Furthermore, the crest of the surface elevation is overestimated from the first measurement location (50.9m) to the mid of breaking zone (around 57.5m). Then it is in good match with experimental data afterwards. Besides, the through of experimental surface elevation was matched generally in shoaling zone, while it was slightly overestimated by waves2Foam in breaking zone and inner surf zone. The cross-shore distribution of the wave height is thus larger according to model simulation. Consequently, the Ursell number (panel B in Figure 3.5) by waves2Foam, with NRMSE of 0.19, is broadly larger than experimental data according Eqn. (2.2). Note the cross-shore distribution of the Ursell number is satisfactorily captured. The simulated one diverges from experimental data from 50.9m to approximately 54.0m where the greatest deviation appears. Then the modelled Ursell number continuously converges to experimental data till the last measurement location (62.0m).

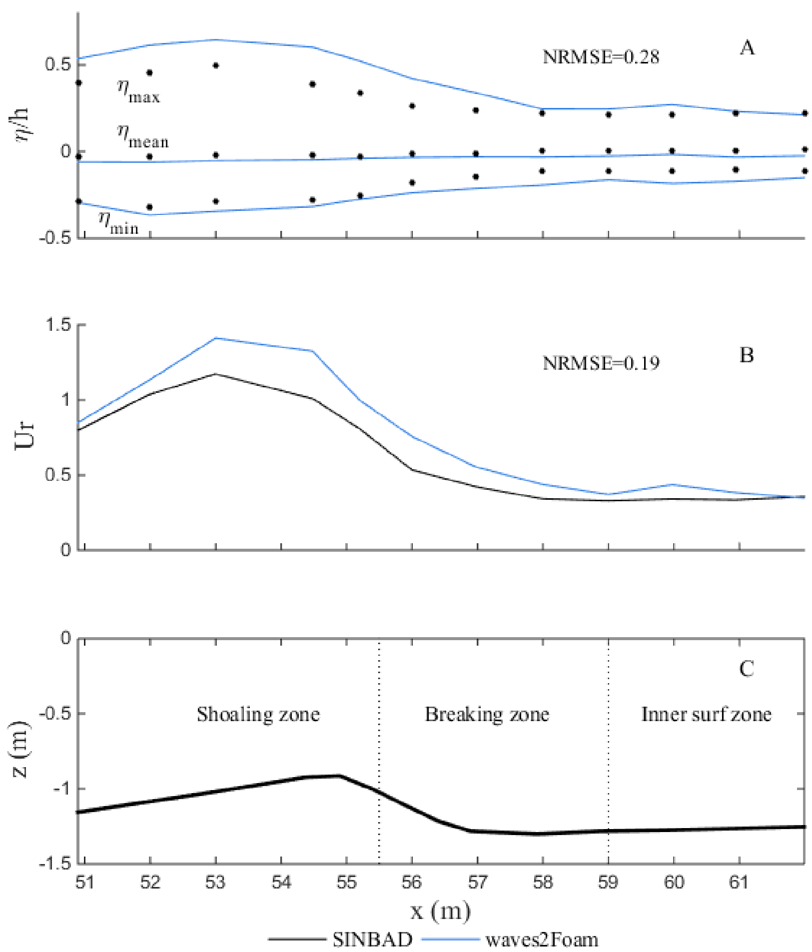

Figure 3.5 The validation in terms of panel A cross-shore surface elevation profiles, and panel B the Ursell number. Blue lines are for waves2Foam simulations. Dark dots and line are for SINBAD data. The normalised root mean square error at measurement locations is represented by NRMSE. Panel C is the measurement area, the thick dark line is the bed profile; the dotted dark lines partition the study region as shoaling zone, breaking zone, and inner surf zone.

3.3 Near-bed orbital velocity

Figure 3.6 compares the dimensionless near-bed orbital velocity among experimental data, model simulation, and Ruessink parameterisation. NRMSE (Eqn. 3.1) is also applied.

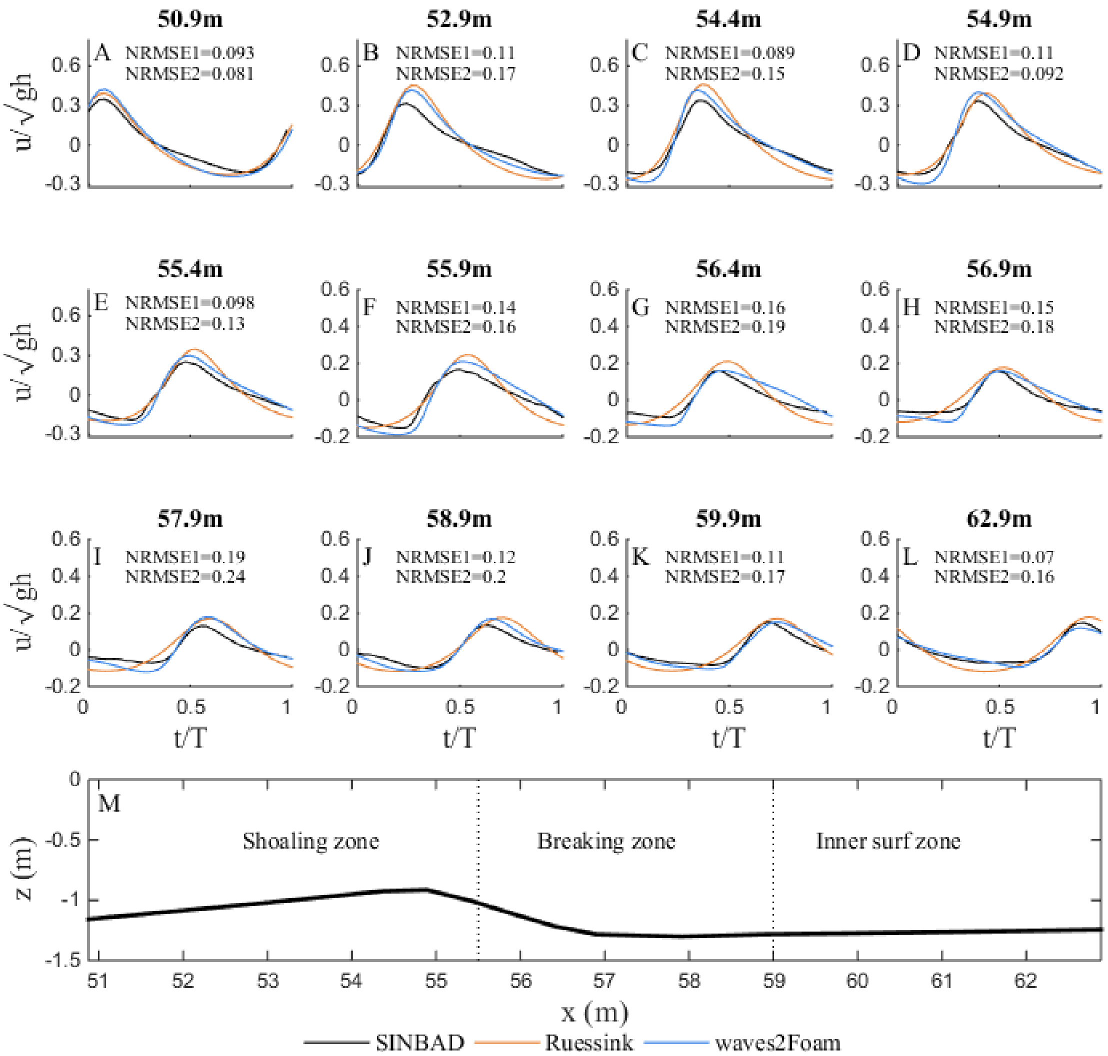

Figure 3.6 Comparing dimensionless phase-averaged near-bed orbital velocity among waves2Fom, SINBAD data, and Ruessink parameterisation. Panels A to L indicate the locations of lower ADVs. The normalised root mean square error of waves2Foam and Ruessink parameterisation are represented by NRMSE1 and NRMSE2. Panel M is the measurement area, the thick dark line is the bed profile; the dotted dark lines partition the study region as shoaling zone, breaking zone, and inner surf zone.

According to the root mean square error of model simulation (NRMSE1), the most mismatches of model simulation occur between 50.9m and 54.9m with average RMSE1 of 0.17. Furthermore, after breaking point (55.5m), the simulated velocity shapes are acceptable with gradually decreasing RMSE1 which is from 0.14 at 55.9m to 0.053 at

62.9m which is the best prediction. Then, the root mean square error of Ruessink parameterisation (NRMSE2) indicates the greatest deviations of velocity shapes at 52.9m and 54.4m with NRMSE2 of 0.29 and 0.24 respectively. The prediction error of Ruessink parameterisation fluctuates after (including) 55.4m moderately with mean RMSE2 of approximately 0.16. Similarly to waves2Foam, the best prediction of Ruessink parameterisation appear at 62.9m with its minimum RMSE2 of 0.12. Comparing NRMSE1 with NRMSE2, Ruessink parameterisation shows slightly better prediction capacity than waves2Foam at 50.9m where NRMSE1=0.17, NRMSE2=0.15, and 55.9m where RMSE1=0.18, RMSE2=0.15. However, for other locations, there is no doubt that waves2Foam overweighs Ruessink parameterisation regarding NRMSE, which basically means that the prediction of waves2Foam matches more the pointwise experimental data. Additionally, comparing NRMSE of modelled surface elevation (Figure 3.4) to NRMSE of modelled near-bed orbital velocity (Figure 3.6), the later matches better the observations at corresponding measurement locations.

Panel A in Figure 3.7 illustrates the comparisons of cross-shore velocity profiles. Both models perform satisfactorily in terms of the prediction of velocity maximum, minimum, and mean. They predict the cross-shore trends of the velocity profiles with few mismatches, e.g. the overestimation of maximum in shoaling zone. The profile of experimental mean velocity is nicely matched, and profiles of both models are overlapped. Note that although waves2Foam and Ruessink parameterisation compute similarly in terms of the velocity profiles (NRMSE1=0.16, NRMSE2=0.18), waves2Foam is still more reliable to predict regular waves. As can be seen from the velocity shapes in Figure 3.6, waves2Foam captures the cross-shore shape transformation, while Ruessink parameterisation computes inaccurate peak and trough time points especially in the region after the breaking point. As results, firstly, in panel B of Figure 3.7, although Ruessink parameterisation shows similar NRMSE (0.33) with waves2Foam (0.35), it varies in a relatively small range between 0.4 and 0.6, and completely cannot follow the cross-shore trend of skewness under regular waves. Comparing with Ruessink parameterisation, waves2Foam predicts better in shoaling and breaking zones, while gives similarly poor results in inner surf zone. Despite waves2Foam simulates smaller and shifted peak value of skewness in breaking zone, it qualitatively captures the fluctuating cross-shore trend of skewness. Secondly, it can be seen in panel C of Figure 3.7 that experimental asymmetry firstly goes down to the lowest points, then reaches the peak point in breaking zone at similar location with skewness (57.0m). Afterwards, it has the same trend as skewness. For waves2Foam, the prediction capacity regarding asymmetry (NRMSE=0.38) is similar with skewness (NRMSE=0.35). And, waves2Foam acceptably captures the varying cross-shore trend of asymmetry. It can be noticed that waves2Foam prediction is corresponding shifting probably due to the slightly shifted peak skewness (panel B). In addition, Ruessink parameterisation results in relatively large NRMSE of 1.1, because it heavily underestimates the asymmetry of regular waves in the study region, also it cannot predict the fluctuating cross-shore trend.

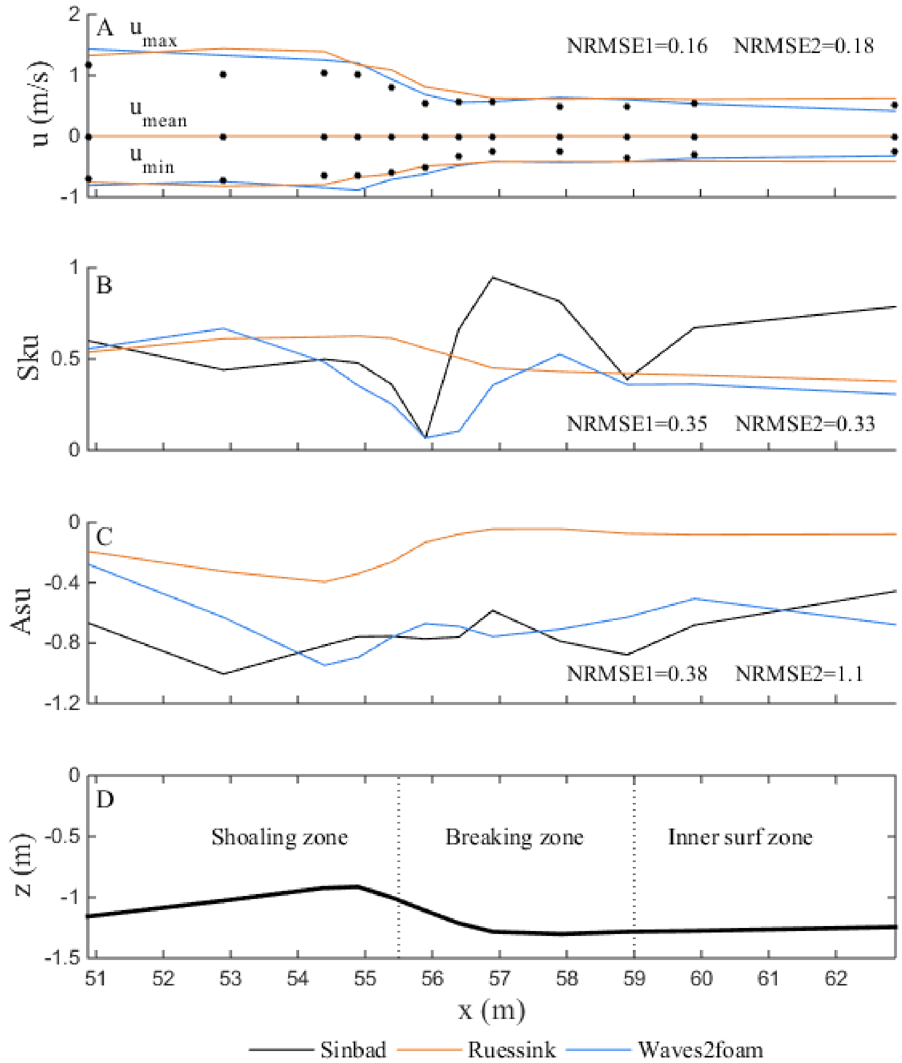

Figure 3.7 The validation in terms of the near-bed orbital velocity panel A cross-shore profiles, panel B skewness, and panel C asymmetry. The normalised root mean square error at measurement locations of waves2Foam and Ruessink parameterisation are represented by NRMSE1 and NRMSE2. Panel C is the measurement area, the thick dark line is the bed profile; the dotted dark lines partition the study region as shoaling zone, breaking zone, and inner surf zone.

3.4 Turbulence

The time-averaged turbulence vertical profile is evaluated in this section. The mean profiles of turbulence at all measurements points are larger than the profiles provided by ADVs. Also, the ADV observation is not always inside the simulated profile envelopes at some measurement locations. The overestimation of time-averaged turbulence profiles is common phenomenon for this kind of turbulence model (see Brown *et al.* 2016).

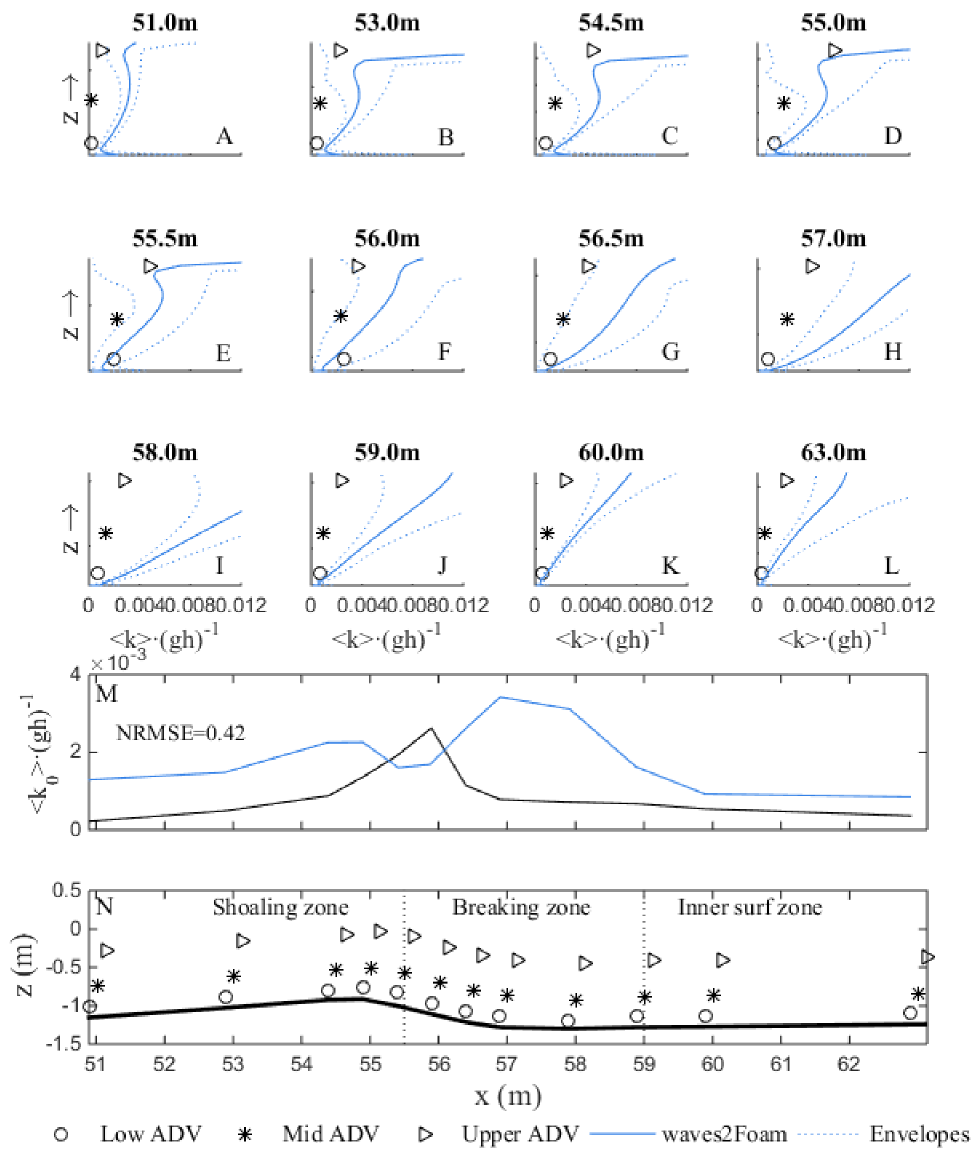

Figure 3.8 Comparing dimensionless time-averaged turbulence along water column between waves2Fom and SINBAD data. Panels A to L indicate the average cross-shore location of ADVs. Panel M is the comparison of time-averaged near-bed turbulence between model simulation and the measurements from lower ADVs. Panel N is the measurement area, the thick dark line is the bed profile; the dotted dark lines partition the study region as shoaling zone, breaking zone, and inner surf zone.

Regarding the experimental measurements, the time-averaged turbulence increases as ADV is closer to the water surface. Moreover, the time-averaged turbulence profile rises from 51.0m to 57.0m then drops gradually. Model waves2Foam captures the trend of rising in x- and z-direction respectively in qualitative way. In x-direction perspective, focusing on the mean vertical profile, the simulated turbulence experiences the same evolution as experimental turbulence. According to the profiles, the modelled turbulence increases from 51.0m to 58.0m and reaches the peak, while the peak of experimental profile is at 57.0m. In z-direction perspective, the overestimation is common at mid and upper ADVs, and it becomes heavier at upper ADV due to the intense water-air interaction. Throughout the study region, the simulated time-averaged turbulence is the more reliable at lower ADVs than mid and upper ADVs, because it overall is the closest to the near-bed observation. Concerning the time-averaged near-bed turbulence in panel M of Figure 3.8, waves2Foam broadly overestimates the values with NRMSE of 0.42 which is relaticely larger comparing with the Ursell number in panel B of Figure 3.5 (NRMSE=0.19), skewness in panel B (NRMSE=0.35) and in panel C asymmetry (NRMSE=0.38) of Figure3.7. Still, waves2Foam qualitatively simulates the correct cross-shore profile of the time-averaged near-bed turbulence. Additionally, it is observable in panel M that a same landwards shifting for modelled data. This shifting is coincident with other cross-shore trends like skewness (panel B in Figure 3.7), asymmetry (panel C in Figure 3.7), and vertical turbulence profiles (panel A to L in Figure 3.8). And the phenomenon of shifting can be seen as a result of that waves2Foam predicts slightly landwards wave breaking (not shown here).

3.4 Conclusion

The depth-averaged turbulence is applied to determine the hydrodynamics equilibrium of waves2Foam simulation, because it takes longer time to reach equilibrium than surface elevation and near-bed orbital velocity. And the system equilibrium of SINBAD simulation is determined at the 8^{th} wave period.

For the surface elevation, waves2Foam can simulate the shapes and the transformation with acceptable NRMSE. Due to the limitation of surface tracking technique, overestimation of crest profile occurs from shoaling zone to the mid of breaking zone. Moreover, the overestimation of trough profile occurs in breaking and inner surf zone. Consequently, the simulated Ursell number is slightly larger than experimental data, but in correct cross-shore trend. The surface variables are satisfactorily simulated in general.

Under the condition of regular waves, Ruessink parameterisation has similar prediction capacity with waves2Foam in terms of near-bed orbital velocity maximum, minimum, and mean. However, according to NRMSE, Ruessink parameterisation matches poorer the observed velocity shapes than waves2Foam simulation. Moreover, it fails to predict correct peak and trough time points hence shape transformation, while waves2Foam does much better. Therefore, waves2Foam overweighs Ruessink parameterisation regarding the prediction of skewness (in shoaling and breaking zones) and asymmetry for regular waves.

As the drawbacks of the applied turbulence model, waves2Foam constantly overestimates the vertical time-averaged turbulence profiles. Comparing among the time-averaged turbulence at different positions of ADVs, the near-bed data is more reliable with the least overestimation. Qualitatively, waves2Foam correctly simulates the development of time-averaged turbulence profiles both vertically and horizontally. Also, it captures cross-shore development of the time-averaged near-bed turbulence. The time-averaged turbulence is less satisfactorily validated. Nonetheless, the more important thing is that the qualitatively correct cross-shore trend is captured (also for other validated variables). This is good enough, as this research focuses more on cross-shore trend. Therefore, waves2Foam can be applied in this research to generate wave data.

Chapter 4

Dependencies analysis

Alike to model validation, this chapter starts with the determination of hydrodynamics equilibrium which facilitate select more periodic wave data for research (Section 4.1). Then, the dependencies of near-bed skewness and asymmetry on chosen physical parameters are presented in the order: wave height (Section 4.2); wave length (Section 4.3); the Ursell number (Section 4.4); surf similarity (Section 4.5); energy dissipation (Section 4.6) which includes wave energy dissipation, roller dissipation, and dissipation by bed friction; and near-bed turbulence (Section 4.7). Moreover, depending on different situations, fittings of dependencies are shown to indicate the simplest linear/non-linear relations between near-bed skewness and asymmetry and physical parameters.

4.1 Hydrodynamics equilibrium

It is clarified in Section 3.1 of Chapter 3 that, depth-averaged turbulence is introduced to determine the hydrodynamics equilibrium of model simulation, because it takes longer time to reaches equilibrium than surface elevation and near-bed orbital velocity. For linear beds simulations, waves2Foam was stable and simulated runtime of 120s for each case, i.e. 30 waves in total.

Taking case H05T4-SL15 as an example, Figure 4.1 shows the time-dependent depth-averaged turbulence from the 10^{th} wave period to the 30^{th}. It can be seen in shoaling zone that, from 40.0m to 46.0m the depth-averaged turbulence reaches the equilibrium at the 15^{th} wave period, while at the 20^{th} wave period at 49.0m and 52.0m. In the breaking zone (55.0m) and inner surf zone (58.0m and 60.0m), the minimum of depth-averaged turbulence remains after the 15^{th} wave period, while the maximum is affected by breaking processes somehow and still fluctuates. However, the maximum at 55.0m varies in relatively small range and can be seen as equilibrium. Moreover, in the inner surf zone, the local peaks of upper envelopes are more or less periodic, and are accepted as equilibrium in this research. For instance, at the most dynamic location 58.0m, the local peaks are approximately at the 18^{th}, 24^{th} and 28^{th} wave period. Thus, adding the consideration the equilibrium in shoaling and breaking zones, the equilibrium of depth-averaged turbulence hence the water system is chosen at the 20^{th} wave period. Namely, 10 waves are selected for dependencies analysis. Furthermore, the 20^{th} wave period is also considered as when the equilibrium is reached for other cases. The corresponding figures about time-dependent depth-averaged turbulence are given in Appendix A.

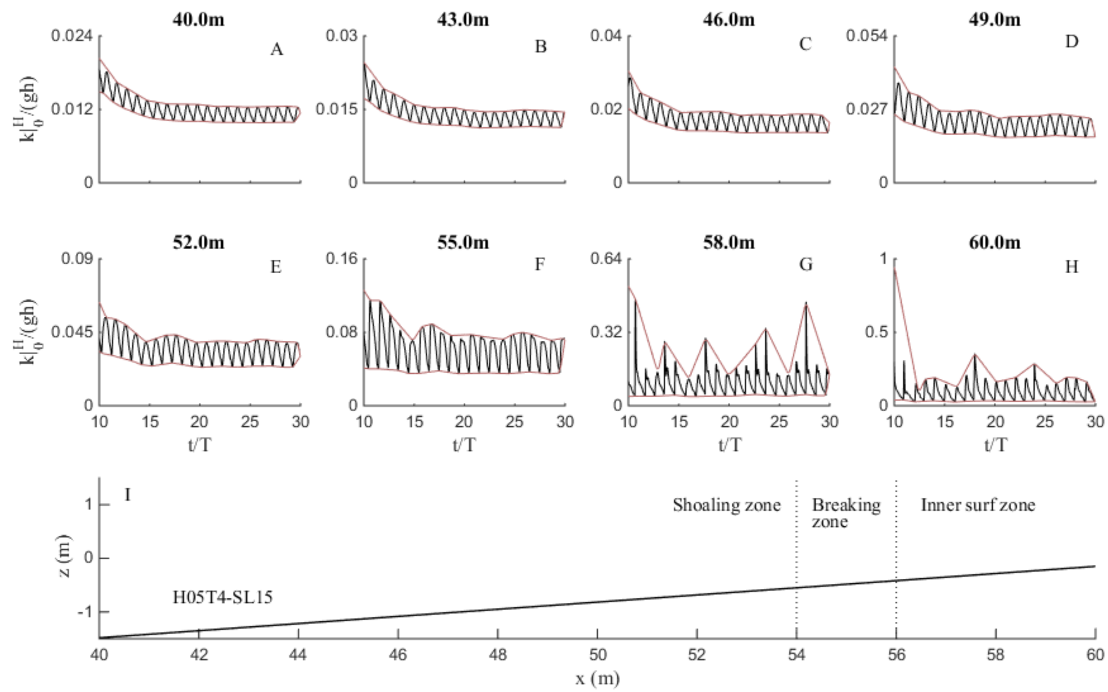

Figure 4.1 Dimensionless depth-averaged turbulence as a function of time of case H05T4-SL15. The light red lines are the envelopes. Panels A to L are measurement locations in the cross-shore order. Panel M is the measurement area, the thick dark line is the bed profile; the dotted dark lines partition the study region as shoaling zone, breaking zone, and inner surf zone.

4.2 Wave height

Figure 4.2 shows the dependencies of skewness and asymmetry on dimensionless wave height. Regarding wave H05T4, it can be seen in panel A that the dependencies of *Sku* on *H/h* in shoaling and breaking zones are irregular for all bed slopes. The dependencies for all slopes are in similar trends that *H/h* gradually increases, while *Sku* alternatingly increases and decreases. But, for steeper bed slope, *Sku* reaches it first peak with larger increment of *H/h* from the first location in the shoaling zone. e.g., value of *H/h* related to the dependencies for SL15, SL20, and SL25 starts at ~0.26, ~0.28, and ~0.3 respectively, and rises to ~0.29, ~0.52, and ~0.58 when *Sku* increases to its first peak value. The dependencies for steeper bed slope is shifted both vertically and horizontally, comparing the one for gentler bed slope. Nevertheless, the dependencies for all bed slopes alternately cross each other and can be described by a general non-linear fit. In terms of the dependencies in inner surf zone in panel B, the dependencies are separated by different bed slopes. However, *Sku* does not depend on *H/h* in this region, because *Sku* drops rapidly while *H/h* is nearly constant for different bed slopes respectively. Panel C displays the dependencies of *Asu* on *H/h* for H05T4 in shoaling and breaking zones. The non-linear dependencies for all bed slopes still can be clearly observed. It can be seen that the maximum *Asu* on steeper bed slope is larger, which are approximately 1.0 for SL25, 1.2 for SL20, and 1.25 for S15. It is evident that the dependencies for different bed slopes are overlapping to large extent. They consequently cluster with linear trend. In panel D, as the dependencies of *Asu* on *H/h* tend to collapse, there is no interesting dependencies can be seen.

About H08T4, the similar dependencies with slope effect can be observed in shoaling and breaking zones. In panel E, *Sku* depends on *H/h* for all bed slopes are irregular, with the first at (0.4, 0.4) for SL15, (0.6, 0.62) for SL20, and (0.7, 0.8) for SL25 approximately.. The dependencies for all bed slopes are slightly away from each other, but they still alternately cross to each other. As a result, non-linear fit can acceptably represent the general relation of them, however with smaller R^2 (0.65) than H05T4 one which is 0.71. In panel G, the dependencies of *Asu* on *H/h* for all bed slopes are slightly scattered than H05T4 in panel C. Nevertheless, they still cluster with clear linear trend. In addition, there are no significant dependencies can be found for *Sku* and *Asu* in the inner surf zone respectively.

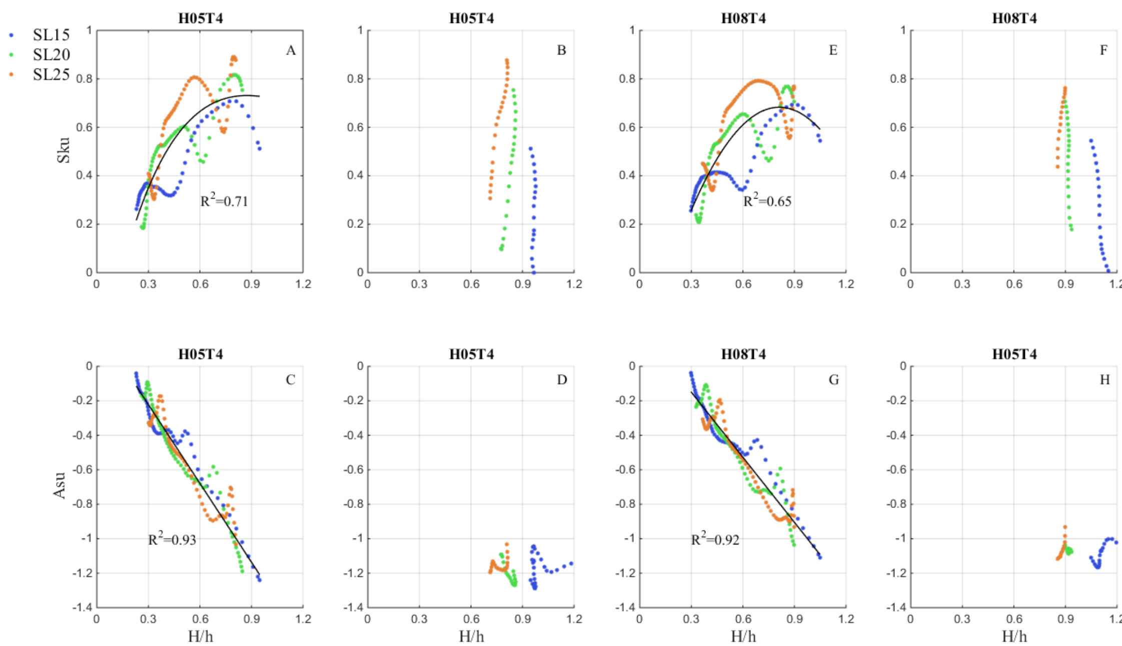

Figure 4.2 Near-bed orbital velocity skewness (*Sku*) and asymmetry (*Asu*) as functions of dimensionless wave height (*H/h*) of cases H05T4 and H08T4. Panel A, C, E, and G are the dependencies in shoaling and breaking zones of corresponding cases. Panel B, D, F, and H are the dependencies in inner surf zone of corresponding cases. The dark curves/lines are the fittings, with coefficient of determination R^2.

4.3 Wavelength

Figure 4.3 shows the dependencies of skewness and asymmetry on dimensionless wavelength. Focusing on H05T4 firstly, the dependencies for all bed slopes in shoaling and breaking zones are alike to *Sku* against *H/h* in panel A of Figure 4.2, which shows *Sku* develops in fluctuating trend with increasing depended *L/h*. Additionally, the first peak value of *Sku* is related to larger *L/h* for gentler bed slope, e.g., roughly, (12, 0.36) for SL15, (15, 0.6) for SL20, and (16, 0.8) for SL25.

However, *Sku* against *L/h* seems like the horizontally compressed *Sku* against *H/h*. It can be therefore fitted by linear function. While in the inner surf zone, panel B displays the three clearly linear dependencies for different bed slopes respectively. Moreover, *Sku* depends on *L/h* in panel B in an opposite trend against it in panel A. i.e., *L/h* is positively correlated to *Sku* in shoaling and breaking zone, while negative correlation is found in inner surf zone. In panel C, it can be observed that the pointwise dependencies for all bed slopes are tightly closed to each other, and cluster to a nearly linear line. And in panel D, *Asu* in inner surf zone does not depend on *L/h*, as it tend to remain with changing *L/h*.

It can be seen from panel E respectively that, the dependencies of *Sku* on *L/h* for the same bed slope are alike to H05T4 in panel A. The pointwise dependencies for H08T4 for all bed slopes are more scattered, which still can be acceptably described by a linear function. This can be also observed when comparing *Asu* against *L/h* between H08T4 (panel G) and H05T4 (panel C). In the inner surf zone, showing the opposite trend against shoaling and breaking zones, *Sku* against *L/h* for H08T4 (panel F) becomes linear and separated by different bed slopes. Still, there are no interesting relations between *Asu* and *L/h* in this region (panel H).

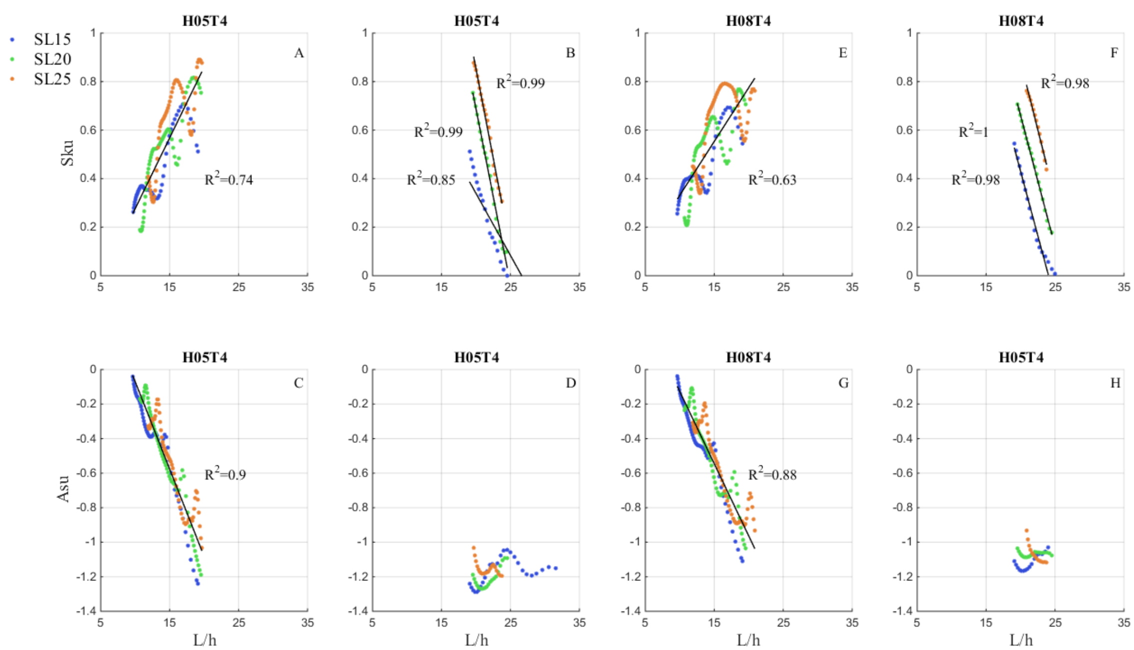

Figure 4.3 Near-bed orbital velocity skewness (*Sku*) and asymmetry (*Asu*) as functions of dimensionless wave length (*L/h*) of cases H05T4 and H08T4. Panel A, C, E, and G are the dependencies in shoaling and breaking zones of corresponding cases. Panel B, D, F, and H are the dependencies in inner surf zone of corresponding cases. The dark lines are the fittings, with coefficient of determination R^2.

4.4 Ursell number

Figure 4.4 displays the relations between the Ursell number and near-bed skewness and asymmetry in whole study regions. Concerning panel A and C, it can be seen that the ranges of *Ur* are slight different, which are from ~0.2 to ~ 11, while from ~0.25 to ~14 for H05T4 and H08T4 respectively. Moreover, H08T4 shows the trend of *Sku* against *Ur* which is planner with smaller peak *Sku*. Furthermore, unlike *H/h* and *L/h*, the relations between *Sku* and *Ur* is not more scattered for H08T4. Instead, the bed slopes effects on both wave conditions are equal. Consequently, the dependencies of different wave conditions are fitted with the same R^2 (0.8) by high-ordered polynomial functions. Similarly to *Sku*, the dependencies of *Asu* on *Ur* of are influenced by wave height effect in terms of the *Asu* maximum. Namely, *Asu* of H08T4 reaches its peak at larger *Ur* (4.0) than H05T4 which is ~3.3. For both wave conditions, the dependencies are equally well fitted (R^2 of 0.8) by high-ordered polynomial functions. Note that the corresponding fits of *Sku* against *Ur*, and *Asu* against *Ur* are able to cover from shoaling zone to inner surf zone respectively.

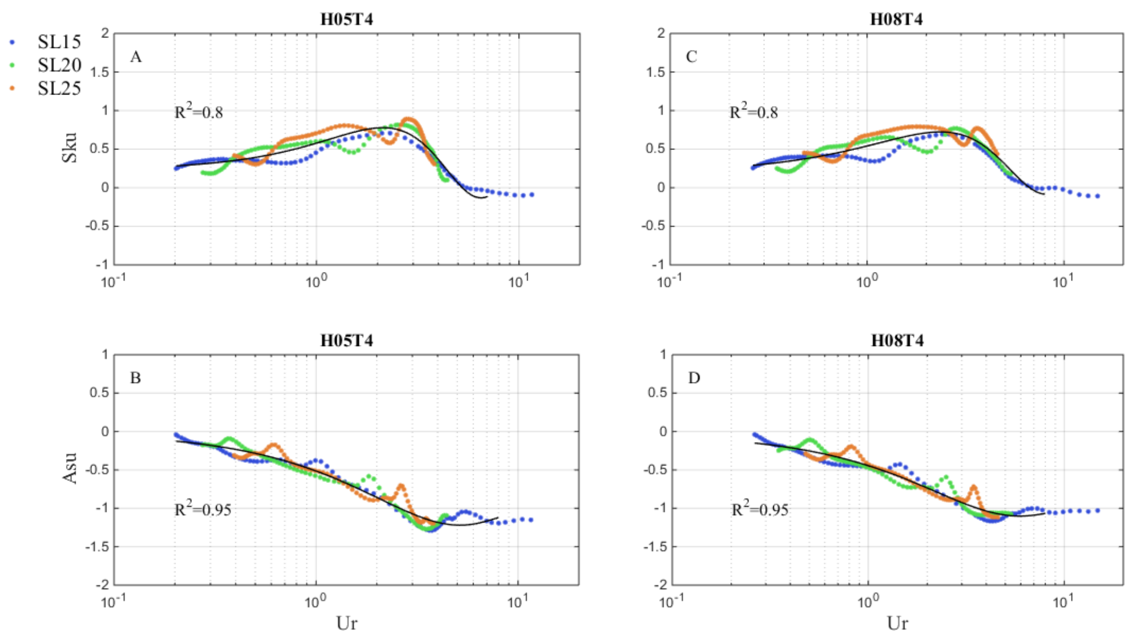

Figure 4.4 Near-bed orbital velocity skewness (*Sku*) and asymmetry (*Asu*) as functions of the Ursell number (U_r). The dark curves are the fittings, with coefficient of determination R^2.

Figure 4.5 compare the dependencies of *Sku* and *Asu* on *Ur* between modelled regular waves of H05T4 on linear beds and field data of irregular waves (see Section 2.2.2) on barred beaches. In panel a, the dependencies of *Sku* broadly fits around the class-mean values of field data. Both data sets are in the same trend which is, with increasing *Ur*, *Sku* gradually increases to the maximum then decreases. However, modelled *Sku* reaches the maximum 0.9 at *Ur* of 4.0, while the class-mean values of observed *Sku* reaches the maximum, ~ 0.7, at *Ur* of 1.0. Moreover, after the point of maximum skewness, it drops quickly and is stable at almost 0 when *Ur* is larger than 7.0, while the observed mean *Sku* goes down slowly and tends to remain at around 0.2 when *Ur* is larger than 9.0. In panel

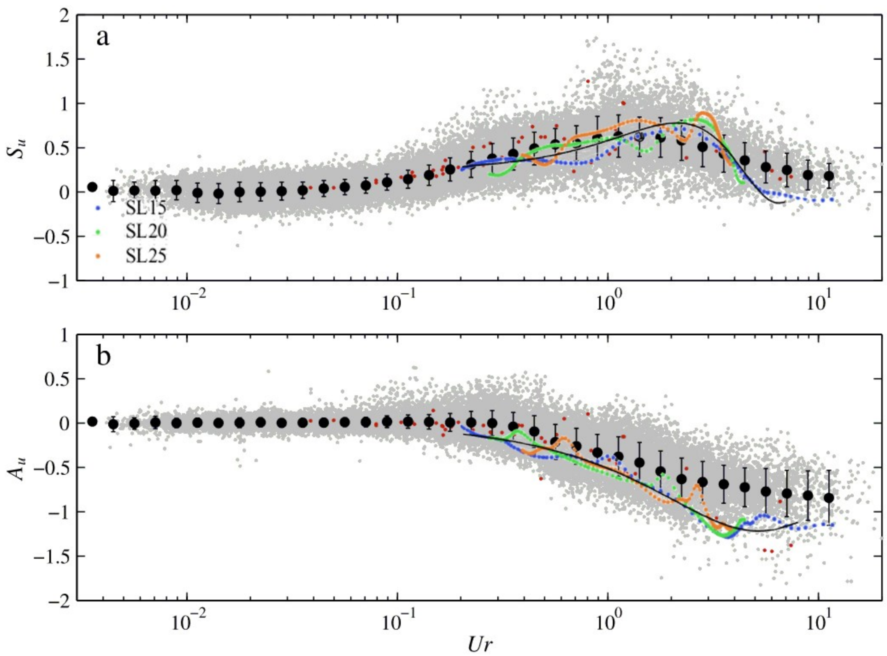

Figure 4.5 Comparisons model results of H05T4 and field data regarding near-bed skewness (*Sku*) and asymmetry (*Asu*) as functions of the Ursell number (U_r). According to Ruessink *et al.* (2012), the grey dots are the individual estimates, in the filled ciecles are class-mean values based on binning the individual estimates according to log(Ur) ±0.05. The vertical lines represent ± one standard deviation in each bin. The red dots are the data of Doering and Bowen (1995)."

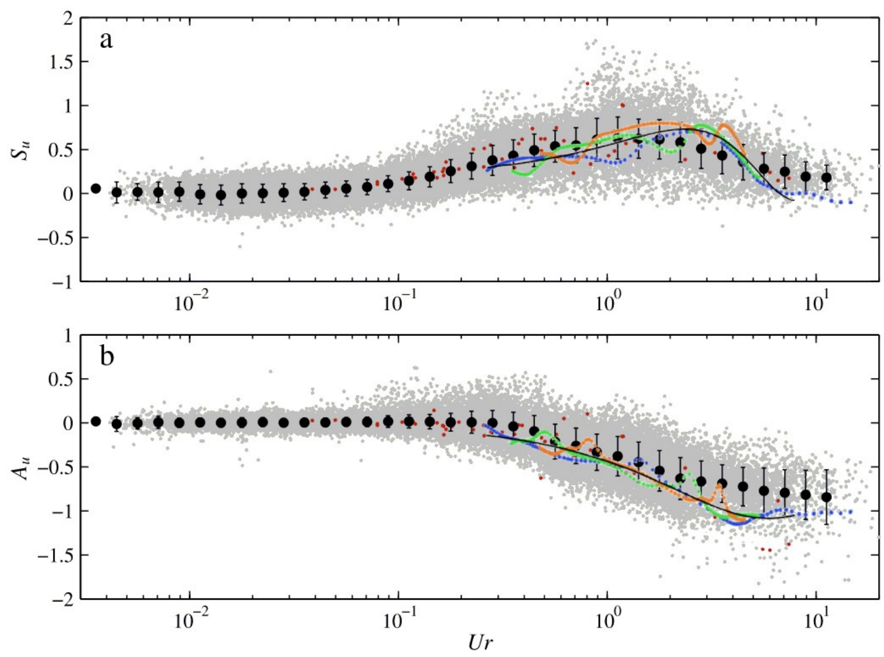

Figure 4.6 Comparisons model results of H08T4 and field data regarding near-bed skewness (*Sku*) and asymmetry (*Asu*) as functions of the Ursell number (U_r). According to Ruessink *et al.* (2012), the grey dots are the individual estimates, in the filled ciecles are class-mean values based on binning the individual estimates according to log(Ur) ±0.05. The vertical lines represent ± one standard deviation in each bin. The red dots are the data of Doering and Bowen (1995)."

b, the dependencies of *Asu* does not well fit the class-mean values of field data. It can be seen that the modelled *Asu* is broadly larger than the class-mean values between *Ur* of 0.2 and 10.0. Besides, the modelled *Asu* experiences the same trend as *Sku*, i.e., with continuously rising *Ur*, *Asu* increases to the maximum (-1.3) then decrease, which is followed by keeping at ~ -1.2 with *Ur* of 7.0. Interestingly, for the dependencies of *Asu* of irregular waves on barred beaches, neither all the individual measurement nor the class-mean values show this trend. Instead, observed class-mean *Asu* rises from 0 at *Ur* of 0.2 to 0.7 at *Ur* of 8.0 approximately, then remains at the same level.

Since the differences of dependencies of *Sku* and *Asu* between H05T4 and H08T4 are subtle (Figure 4.2), the comparisons regarding H08T4 and field data in Figure 4.6 present nearly the same results as H05T4 in Figure 4.5. According to the comparisons in Figure 4.4 and 4.5, it can be thus said that for the regular waves on linear beds, *Sku* and *Asu* is related to *Ur* differently with irregular waves on barred beds to some extent.

4.5 Surf similarity parameter

The dependencies of near-bed skewness and asymmetry on surf similarity parameter are presented in Figure 4.7. The bed slope effect on the dependencies in Figure 4.7 is significant throughout the study area. There is no overlapping among the pointwise dependencies for different slopes in each panel of Figure 4.7. Therefore, in each panel, the dependencies for different bed slopes can only be fitted respectively, and no general fit can be obtained. For instance, about H05T4, panel A displays that the separated dependencies for different bed slopes are fitted by different linear lines respectively. These linear trend lines are resolved best fits, but they cannot adequately represent the irregular pointwise dependencies. In inner surf zone (panel B), the dependencies for different bed slopes become linear and parallel to each other with the coincident trend with shoaling and breaking zones. In panel C, the dependencies of *Asu* on ξ for different bed slopes are acceptably represented by the linear fits respectively. As can be seen from the fits in panel A and C, the fit for SL25 is the steepest, which means that both *Sku* and *Asu* are more sensitive to the change of ξ on gentler bed slope. Under the same case, the dependencies of *Sku* and *Asu* for H08T4 are correspondingly alike to H05T4. The wave height effect can be viewed more clearly in the shoaling and breaking zones. For the same bed slope, say SL15, the *Sku* against ξ between H05T4 (panel A) shows a milder trend than H08T4 (panel E), which indicates that the dependencies is more sensitive to waves with higher *H*.

Despite the dependencies in Figure 4.7 are clear and can be simply fitted, they are not favourable for parameterisation. Because, firstly the relations between *Sku* and ξ are irregular and cannot be described by linear fits properly; secondly, strong bed slope effect makes situation complicated, i.e., the parameterisation (if there were) has the limitation about the validity regime. However, it is still a good parameter for one who wants to incorporate the bed slope effect in parameterisation.

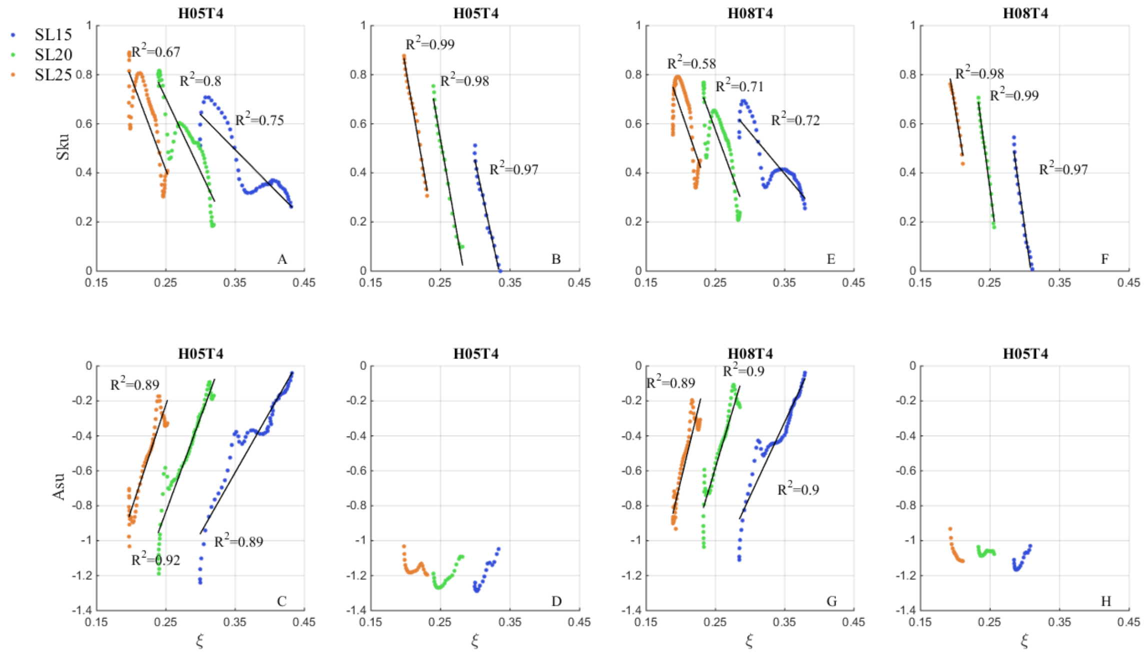

Figure 4.7 Near-bed orbital velocity skewness (*Sku*) and asymmetry (*Asu*) as functions of surf similarity (ξ) of cases H05T4 and H08T4. Panel A, C, E, and G are the dependencies in shoaling and breaking zones of corresponding cases. Panel B, D, F, and H are the dependencies in inner surf zone of corresponding cases. The dark lines are the fittings, with coefficient of determination R^2.

4.6 Energy dissipation

4.6.1 Wave energy dissipation

The relations between the dimensionless D_w and *Sku* and *Asu* are presented in Figure 4.8. It can be seen from panel A and B that all points are scattered to large extent for H05T4 and H08T4 respectively. Consequently, no relations can be found between *Sku* and D_w $(U_w^3\rho)^{-1}$. In panel C and D, there are relations between *Asu* and $D_w(U_w^3\rho)^{-1}$ can be seen for H05T4 and H08T4 respectively. *Asu* is related to D_w $(U_w^3\rho)^{-1}$ in non-linear trend somehow which can be fitted well by none of the fitting techniques in this research. So the trend lines given in panel C and D merely indicate the rough negative correlations between *Asu* and D_w $(U_w^3\rho)^{-1}$.

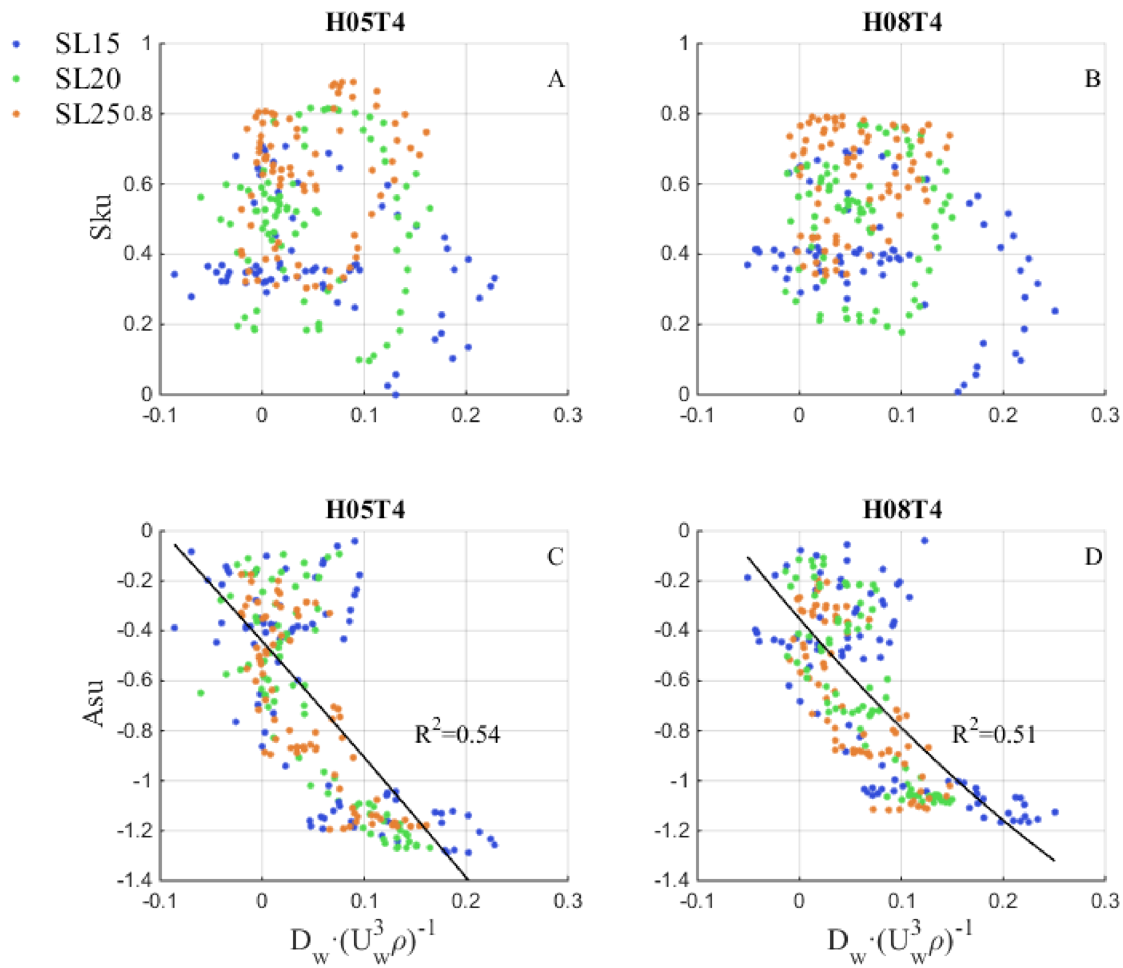

Figure 4.8 Near-bed orbital velocity skewness (*Sku*) and asymmetry (*Asu*) as functions of dimensionless wave energy dissipation ($D_w\ (U_w^3\rho)^{-1}$) of cases H05T4 and H08T4. The dark curves/lines are the fittings, with coefficient of determination R^2.

4.6.2 Roller dissipation

The dependencies of skewness and asymmetry on dimensionless roller dissipation are presented in Figure 4.9. Since $D_r\ (U_w^3\rho)^{-1}$ is a turbulence related term and independent from basic wave parameters, there are some new non-linear dependencies of *Sku* and *Asu* on $D_r\ (U_w^3\rho)^{-1}$ shown in shoaling and breaking zones. For H05T4, it can be observed from panel A and C that no slope effect appears. Furthermore, the fits satisfactorily describe that *Sku* and *Asu* exponentially decay with increasing $D_r\ (U_w^3\rho)^{-1}$ in panel A and C respectively. While in inner surf zone, the relations between *Sku* and $D_r\ (U_w^3\rho)^{-1}$ becomes relatively linear for all different bed slopes. While *Asu* does not depend on $D_r\ (U_w^3\rho)^{-1}$ in this region, because $D_r\ (U_w^3\rho)^{-1}$ here varies in very small range (between 0 and ~0.3×10^{-4}) and *Asu* is almost constant. Since the relations between *Asu* and $D_r\ (U_w^3\rho)^{-1}$ in inner surf zone contains very small weight among the pointwise dependencies in whole study area, they could be neglected for fitting. Therefore, the fit in panel C can be considered to be able to represent dependencies of *Asu* on $D_r\ (U_w^3\rho)^{-1}$ from shoaling zone to inner surf zone.

Comparing with H05T4, the pointwise dependencies of *Sku* and *Asu* for H08T4 in shoaling and breaking zones are more scattered, as result they are fitted exponentially with smaller R^2. The fit in panel G could be used to describe the *Asu* against $D_r\ (U_w^3\rho)^{-1}$ in whole study area, for the same reason as H05T4. Moreover, in shoaling and breaking zones, *Sku* (*Asu*) for H05T4 exponentially decay with increase $D_r\ (U_w^3\rho)^{-1}$ than H08T4. Besides, in inner surf zone, the trends of *Sku* against $D_r\ (U_w^3\rho)^{-1}$ for H05T4 are broadly steeper than H08T4. Hence, it can be said that *Sku* (*Asu*) is more sensitive to the change of $D_r\ (U_w^3\rho)^{-1}$ for the waves with smaller *H*.

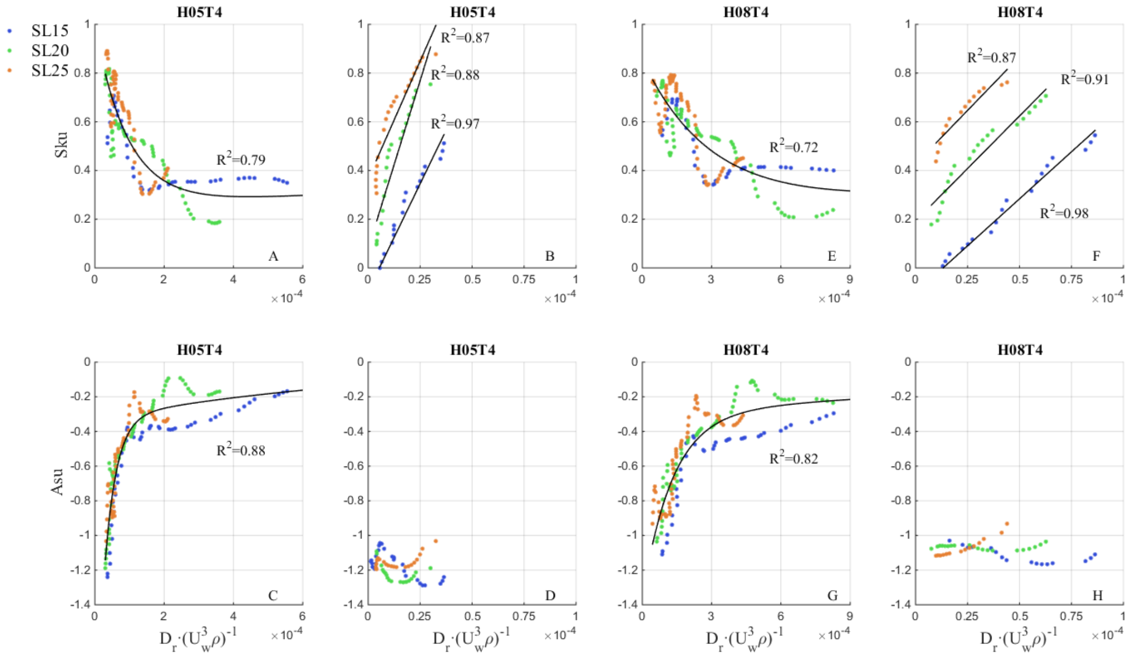

Figure 4.9 Near-bed orbital velocity skewness (*Sku*) and asymmetry (*Asu*) as functions of dimensionless roller dissipation ($D_r\ (U_w^3\rho)^{-1}$) of cases H05T4 and H08T4. Panel A, C, E, and G are the dependencies in shoaling and breaking zones of corresponding cases. Panel B, D, F, and H are the dependencies in inner surf zone of corresponding cases. The dark curves/lines are the fittings, with coefficient of determination R^2.

4.6.3 Dissipation due to bed friction

Figure 4.2 illustrates the dependencies of near-bed skewness and asymmetry on dissipation due to bed friction. It can be seen in shoaling and breaking zones, the dependencies of *Sku* and *Asu* on $D_f\ (U_w^3\rho)^{-1}$ are alike to the dependencies on *H/h* (Figure 4.2) and on *L/h* (Figure 4.3) to some extent. However, the dependencies on $D_r\ (U_w^3\rho)^{-1}$ are more complex and irregular so that their trends are less clear. For example, in panel A, the dependencies for different bed slopes converge at point (0.8×10^{-3}, 0.3), then they diverge with increasing *Sku* and $D_f(U_w^3\rho)^{-1}$ in very curvy ways respectively. And the dependencies are more sensitive on gentler bed slope. The R^2 of the fits for different bed slopes seems to be acceptable (0.79 for SL15, 0.81 for SL20, 0.61 for SL25).Yet, the linear fits cannot represent properly the relations between *Sku* and $D_f\ (U_w^3\rho)^{-1}$. Instead, they can merely indicate the very rough positive correlation. This can be also observed in panel C. The dependencies for different bed slopes start at around point (0.8×10^{-3}, -0.1), then diverge with increasing $D_f\ (U_w^3\rho)^{-1}$. However, they show the linear trend at very beginning from the starting point, then they gradually lose the linearity and become bent, especially for SL15. The above situation can be also seen from the corresponding dependencies for H08T4. Thus, it is obvious that the dependencies in Figure 4.10 is not favourable for parameterisation.

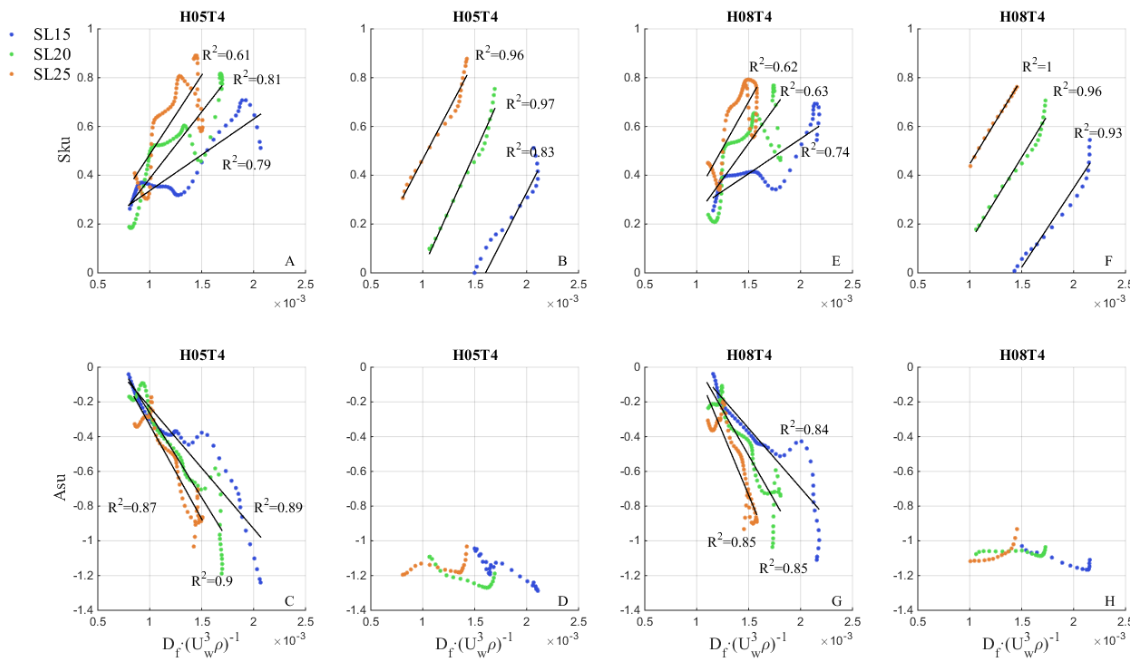

Figure 4.10 Near-bed orbital velocity skewness (*Sku*) and asymmetry (*Asu*) as functions of dimensionless dissipation due to bed friction ($D_f\,(U_w^3\rho)^{-1}$) of cases H05T4 and H08T4. Panel A, C, E, and G are the dependencies in shoaling and breaking zones of corresponding cases. Panel B, D, F, and H are the dependencies in inner surf zone of corresponding cases. The dark lines are the fittings, with coefficient of determination R^2.

4.7 Near-bed turbulence

The dimensionless time-averaged near-bed turbulence is related to near-bed skewness and asymmetry in Figure 4.11. Interestingly, $<k_0>\ (gh)^{-1}$ is an independent parameter from *H*, but it related to *Sku* and *Asu* in a similar way to *H/h*. Comparing panels for shoaling and breaking zones correspondingly in Figure 4.2 and 4.11, the found phenomena for *H/h* are to some extent valid for $<k_0>\ (gh)^{-1}$, in terms of the formations of pointwise dependencies, the first *Sku* peak, bed slope effect, the fits, and etc.. Concerning the region of inner surf zone, the relations between *Sku* and $<k_0>\ (gh)^{-1}$ (panel B and F) are roughly considered as positive correlation for SL25, no dependencies for SL20, and negative correlation for SL15 respectively, which are completely different with the dependencies on all other physical parameters which are in coincident trend in this region. Additionally, it can be seen from panel D and H that the relations between *Asu* and $<k_0>$ $(gh)^{-1}$ in inner surf zone are not interesting. So far, it is common that no favourable relations can be found between *Asu* and one physical parameter in inner surf zone. Under the condition of regular waves on linear beds, $<k_0>$ $(gh)^{-1}$ is related to *Sku* and *Asu* in similar ways to *H/h*. The information of $<k_0>$ $(gh)^{-1}$ probably is embedded in *H/h*. Therefore, *H/h* can be a good alternative to $<k_0>$ $(gh)^{-1}$ for parameterisation.

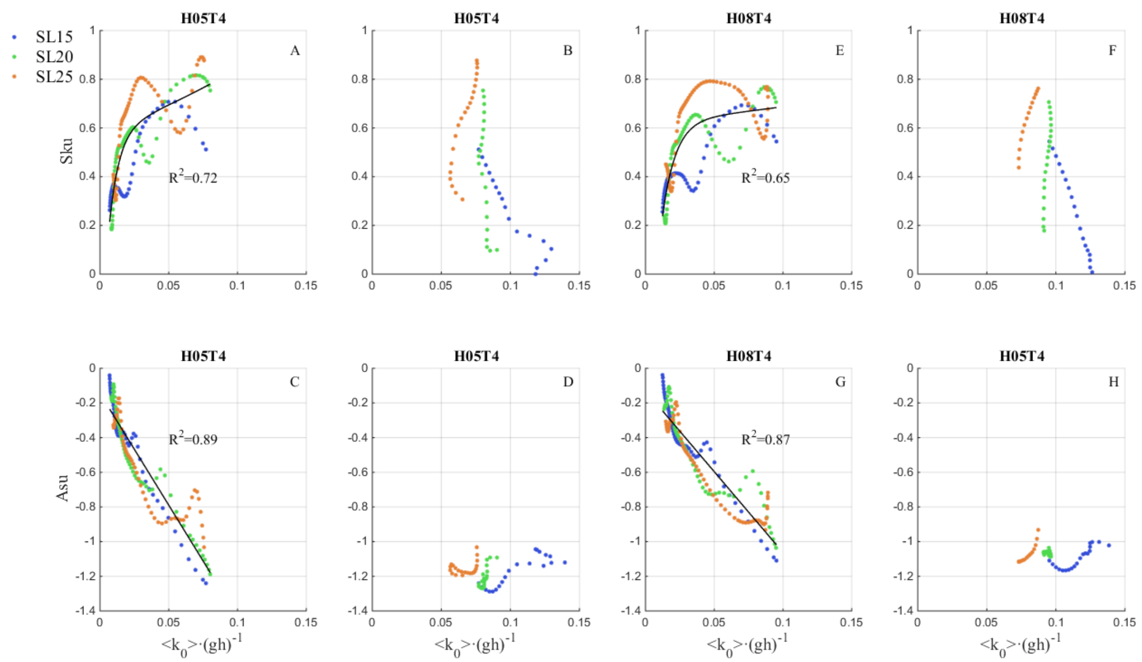

Figure 4.11 Near-bed orbital velocity skewness (*Sku*) and asymmetry (*Asu*) as functions of dimensionless time-averaged near-bed turbulence ($<k_0>$ $(gh)^{-1}$) of cases H05T4 and H08T4. Panel A, C, E, and G are the dependencies in shoaling and breaking zones of corresponding cases. Panel B, D, F, and H are the dependencies in inner surf zone of corresponding cases. The dark curves/lines are the fittings, with coefficient of determination R^2.

4.8 Conclusion

According to the analysis in this Chapter, ξ, $D_w(U_w^3\rho)^{-1}$ and $D_f\,(U_w^3\rho)^{-1}$ are not suitable for parameterisation. Because, firstly, mainly the relations between *Sku* (*Asu*) and ξ depend largely on bed slope, which gives complex validity regime for parameterisation; secondly, there is no relation between *Sku* and $D_w(U_w^3\rho)^{-1}$ due to highly scattered pointwise dependencies. Moreover, the relation between *Asu* and $D_w(U_w^3\rho)^{-1}$ cannot be satisfactorily fitted. Thirdly, the dependencies of *Sku* and *Asu* on $D_f\,(U_w^3\rho)^{-1}$ in shoaling and breaking zones are too complex and irregular to derive a parameterisation.

The dependencies of *Sku* and *Asu* on the rest physical parameters can be observed and fitted respectively. But note that in inner surf zone, *Asu* does not depend on all of them, but *Ur* and $D_r\,(U_w^3\rho)^{-1}$. Furthermore, $<k_0>$ $(gh)^{-1}$ is related to *Sku* and *Asu* similarly to *H/h*. This is only valid under the condition of regular waves on linear beds (slope bigger than1/25). Thus, as a simpler parameter, H/h is a better choice than $<k_0>$ $(gh)^{-1}$ for parameterisation. Finally, the suggested parameters for further analysis on parameterisation are H/h, L/h, Ur, and D_r $(U_w^3\rho)^{-1}$. And they will be discussed in the next Chapter.

Chapter 5

Discussion

To parameterise near-bed skewness and asymmetry for practical use, there two considerations. On one hand, chosen physical parameter should be related to near-bed skewness and asymmetry in the trend, which can be satisfactorily fitted by relatively simple trend lines. On the other hand, the chosen parameter should be as simple as possible.

Table 5.1 shows R^2 of these dependencies in order to exam and compare how well dependencies of *Sku* and *Asu* on selected parameters can be fitted respectively. Firstly, the general fits can be found to represent the dependencies of *Sku* on a physical parameter for all bed slops in shoaling and breaking zones. The R^2 is ranked as: *Ur*, $D_r\ (U_w^3\rho)^{-1}$, *L/h, H/h*, from high to low, which indicates that it is better to introduce *Ur* or $D_r\ (U_w^3\rho)^{-1}$ in parameterisations of *Sku*, instead of directly using simple parameters *H/h* or *L/h* in this region. Moreover, in inner surf zone, *Sku* does not depend on *H/h*. And, it linearly depends on the $D_r\ (U_w^3\rho)^{-1}$(Figure 4.9), and *L/h* (Figure 4.3) with the slope effects, thus there are three fits for different bed slopes respectively. Furthermore, *Ur* is related to *Sku* in a single non-linear trend without slope effects in whole study region (Figure 4.4).

Secondly, for *Asu*, the dependencies on $D_r\ (U_w^3\rho)^{-1}$, and *Ur* can be described by one function respectively in the whole study region. The dependencies on *H/h* and *L/h* can be fitted satisfactorily respectively, only in shoaling and breaking zones. However, there is nothing interesting between *Asu* and *H/h* and *L/h* respectively in the inner surf zone.

Thirdly, the relations between *Ur* and *Sku* and *Asu* are not influenced by wave height effect. For both H05T4 and H08T4, R^2 keeps at 0.8 for *Sku* and 0.95 for *Asu* respectively.

For the other physical parameters, in shoaling and breaking zones, the fits for the dependencies are better for H05T4 than H08T4 in terms of *Sku* and *Asu* respectively. As shown in corresponding figures in Chapter 4, this is because the pointwise dependencies are more scattered when the input wave height is higher, the fits hence less match them. Moreover, the dependencies of *Sku* on physical parameters is more sensitive to wave height effects than *Asu*. Namely, the differences R^2 regarding dependencies of *Sku* between H05T4 and H08T4 are broadly larger. For instance, R^2 for *Sku* against *H/h* varies from 0.71 for H05T4 to 0.65 for H08T4, while R^2 changes from 0.93 for H05T4 to 0.92 for H08T4 for *Asu* against *H/h*. In inner surf zone, the wave height does not impact on the dependencies.

Table 5.1 The list of R^2 of resolved best fits of the dependencies of *Sku* and *Asu* on chosen physical parameters for all cases. “-” means no interesting dependencies.

<table>
<tr><th></th><th>Wave condition</th><th>Region of</th><th>Bed slope</th><th>H/h</th><th>L/h</th><th>Ur</th><th>$D_r (U_w^3\rho)^{-1}$</th></tr>
<tr><td rowspan="4">Sku</td><td rowspan="2">H05T4</td><td>Shoaling & breaking</td><td>1/15
1/20
1/25</td><td>0.71</td><td>0.74</td><td rowspan="2">0.8</td><td>0.79</td></tr>
<tr><td>Inner-surfing</td><td>1/15
1/20
1/25</td><td>-</td><td>0.99
0.99
0.99</td><td>0.97
0.88
0.87</td></tr>
<tr><td rowspan="2">H08T4</td><td>Shoaling & breaking</td><td>1/15
1/20
1/25</td><td>0.65</td><td>0.63</td><td rowspan="2">0.8</td><td>0.72</td></tr>
<tr><td>Inner-surfing</td><td>1/15
1/20
1/25</td><td>-</td><td>0.98
1.00
0.98</td><td>0.98
0.91
0.87</td></tr>
<tr><td rowspan="4">Asu</td><td rowspan="2">H05T4</td><td>Shoaling & breaking</td><td>1/15
1/20
1/25</td><td>0.93</td><td>0.90</td><td rowspan="2">0.95</td><td rowspan="2">~0.88</td></tr>
<tr><td>Inner-surfing</td><td>1/15
1/20
1/25</td><td>-</td><td>-</td></tr>
<tr><td rowspan="2">H08T4</td><td>Shoaling & breaking</td><td>1/15
1/20
1/25</td><td>0.92</td><td>0.88</td><td rowspan="2">0.95</td><td rowspan="2">~0.82</td></tr>
<tr><td>Inner-surfing</td><td>1/15
1/20
1/25</td><td>-</td><td>-</td></tr>
</table>

According to the above analysis, *Ur*, and $D_r (U_w^3\rho)^{-1}$ are better physical parameters related to *Sku* and *Asu*. And they are potential to be applied in the parameterisation of *Sku* and *Asu* under condition of regular waves propagating on linear beds. The Ursell number is computed from wave height and wave number, so it can be simply applied in parameterisation according the Ruesskin’s work. However, $D_r (U_w^3\rho)^{-1}$ is a complex parameter which is impossible to be directly used in parameterisation. Therefore, Figure 5.1 presents the link between $D_r(U_w^3\rho)^{-1}$ and basic wave parameters. It can be seen in Figure 5.1 that, it is evident that *H/h* and *L/h* are the functions of $D_r(U_w^3\rho)^{-1}$ respectively, i.e. there is the possibility to express $D_r(U_w^3\rho)^{-1}$ with *H/h* and *L/h*. Therefore, a brand-new idea is arouse to include the effect of roller dissipation in the parameterisation of near-bed skewness and asymmetry. This hypothesis is required to be further researched.

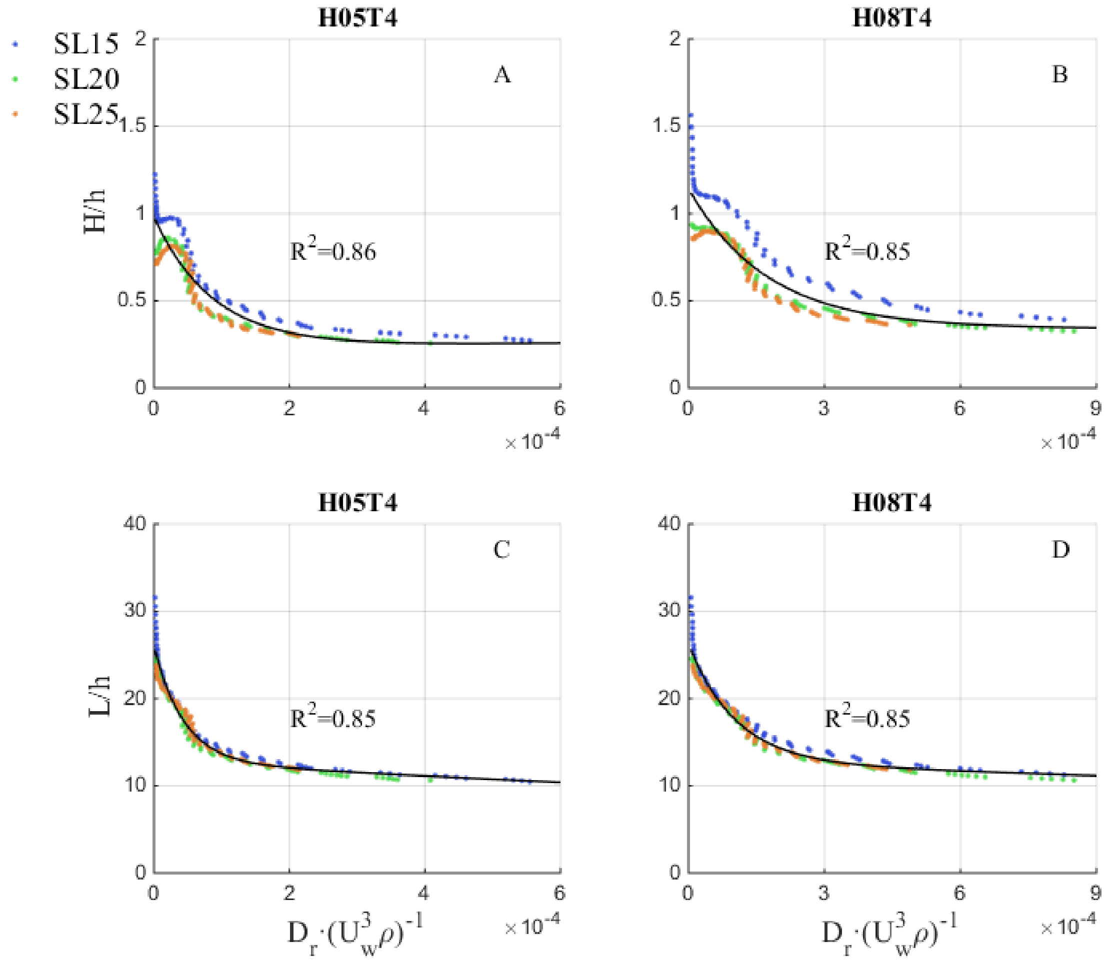

Figure 5.1 Dimensionless wave height (*H/h*) and dimensionless wave length (*L/h*) as functions of dimensionless roller dissipation ($D_r\ (U_w^3\rho)^{-1}$) of cases H05T4 and H08T4 respecticely.The dark curves are the fittings, with coefficient of determination R^2.

Chapter 6
Conclusion and recommendations

6.1 Conclusion

The research objective of this research is presented in Section 1.2. It is:

To determine wave shoaling and breaking effects on the near-bed orbital velocity skewness and asymmetry in order to improve the orbital velocity parameterisation by Ruessink et al. (2012).

Just after the research objective, the research objective, the relative research question and sub-questions are presented in Section 1.2. The objective is achieved by answering the research questions as follow:

How well can wave2Foam simulate near-bed orbital velocity under regular waves?

The observed data from the SINBAD mobile bed CIEM wave flume experiment (H=0.85m, T=4.0s) with barred beach with foreslope of 1/10 is used to validate the numerical model waves2Foam. The surface elevation, near-bed orbital velocity, and turbulence were measured at 12 cross-shore locations from shoaling zone to inner surf zone. Velocity and turbulence were measured at 3 vertical positions at each cross-shore location.

For the surface elevation, waves2Foam can simulate the shapes and the transformation with acceptable NRMSE. But, it overestimation of crest profile occurs from shoaling zone to the mid of breaking zone, while the overestimation of trough profile occurs in breaking and inner surf zone. Consequently, the simulated Ursell number with correct cross-shore trend, is larger than experimental data quantitatively. The surface variables are satisfactorily simulated in general.

Under the condition of regular waves, waves2Foam is able to predicts the near-bed orbital velocity maximum, minimum, and mean broadly. Moreover, the simulated velocity shape matches acceptably the experiment velocity shapes. It is important that it is able to capture the velocity shape transformation. As results, the simulated near-bed asymmetry is satisfactorily validated to experimental data. And, the simulated near-bed skewness is validated from the shoaling zone to the right boundary of breaking zone, while is not validated in inner surf zone.

The waves2Foam constantly overestimates the vertical time-averaged turbulence profiles. Comparing among the time-averaged turbulence at different positions of ADVs, the near-bed data is more reliable with the least overestimation. Qualitatively, waves2Foam correctly simulates the development of time-averaged turbulence profiles both vertically and horizontally. Also, it captures cross-shore development of the time-averaged near-bed turbulence. The time-averaged turbulence is less satisfactorily validated. Nonetheless, the more important thing is that the qualitatively correct cross-shore trend is captured.

Despite waves2Foam simulates the wave with some deviations regarding the values according to the above, it can broadly capture the cross-shore distributions in terms of surf elevation, near-bed skewness and asymmetry, the Ursell number, and etc.. As the cross-shore trend is more important in this research, therefore waves2Foam can be used.

How do wave shoaling and breaking affect the near-bed orbital velocity?

The physical parameters applied in this research are: wave height, wavelength, surf similarity parameter, the Ursell number, wave energy dissipation, roller dissipation, dissipation due to bed friction, and near-bed turbulence. The dependencies of near-bed skewness and asymmetry on wave energy dissipation and dissipation by bed friction are evident respectively, thus they are not favourable for parameterisation. Moreover, the dependencies on surf similarity are strongly influenced by bed slope effect, which results in the dependencies for all the cases need to be fitted respectively.

For the rest physical parameters – wave height, wave length, the Ursell number, roller dissipation, and near-bed turbulence – the bed slope effect is weak on them in shoaling and breaking zones. Thus there are always general trends can be found for these physical parameters respectively. The dependencies on them show steeper trend for H05T4 than H08T4, i.e., both near-bed skewness and asymmetry are more sensitive to depended parameters when wave height is smaller. In inner surf zone, the dependencies of near-skewness on them (except the Ursell number) affected by the bed slope effect and are constantly linear. The near-bed asymmetry only depend on the Ursell number and roller dissipation.

How can the Ruessink parameterisation be improved?

In this research, under the condition of regular waves on linear beds (slope bigger than 1/25), the Ursell number and roller dissipation are selected for parameterisation. It can refer the idea of Ruessink' work to parameterise near-bed skewness and asymmetry by Ursell number, under the condition of regular waves on linear beds with slope bigger than 1/25. Additionally, as the roller dissipation can be expressed by basic wave parameters, like wave height and wavelength. It illustrates the possibility of involving a new process in parameterisation. The potential parameterisation could help Ruessink' method, but it need to be deeper studied.

6.2 Recommendations

A number of recommendations is presented to facilitate an improved Ruessink parameterisation.

Firstly, in terms of the parameterisation, the Ursell number is the first option for as it can be relatively applied in existing Ruessink parameterisation. And, it overweighs other physical parameters in terms of the extent of being influenced by the wave height effect and bed slope effect. Furthermore, it is still in great interests to involve a new physical process in parameterisation in further research. The roller dissipation is possible to be applied in parameterisation, because it is the function of wave height and wavelength respectively, under the condition in this research. However, one should be careful when deriving the parametrisation for near-bed skewness. Because, the dependencies in shoaling and breaking zones are exponential, while linear in inner surf zone. Besides, the dependencies of near-bed skewness and asymmetry of the roller dissipation are influenced by the wave height effect. This could result in a validity regime regarding wave height.

Secondly, the dependencies from six case studies is inadequately to derive a parameterisation. It is suggested to take into account other input wave heights and linear bed (slope smaller than 1/25). It is also important to including other conditions, like long waves, because long waves behave differently with short waves regarding cross-shore distributions of near-bed skewness and asymmetry (Fernandez-Mora. 2015); also the barred beach.

Thirdly, in this research, the accuracy of surface elevation (by the method in Appendix B.1) could be affected to some extent, as well as the relative variables like wave height, the Ursell number, surf similarity, and etc.. Therefore, an improved tracking techniques of free surface is in necessity.

References

Abreu, T., Silva, P. A., Sancho, F., and Temperville, A. (2010). Analytical approximate wave form for asymmetric waves. *Coastal Engineering*, *57*(7), 656-667.

Battjes, J. A. (1974), Surf similarity parameter. *Coastal Engineering Proceedings International Conference on Coastal Engineering*, no.14, 466-480.

Battjes, J. A., and Janssen, J. P. F. M. (1978). Energy loss and set-up due to breaking of random waves. *Coastal Engineering Proceedings*, *1*(16).

Brown, S. A., Greaves, D. M., Magar, V., and Conley, D. C. (2016). Evaluation of turbulence closure models under spilling and plunging breakers in the surf zone. *Coastal Engineering*, *114,* 177-193.

Christensen, E. D., and Deigaard, R. (2001). Large eddy simulation of breaking waves. *Coastal engineering*, *42*(1), 53-86.

Drake, T. G., and Calantoni, J. (2001). Discrete particle model for sheet flow sediment transport in the nearshore. *Journal of Geophysical Research: Oceans*, *106*(C9), 19859-19868.

Doering, J. C., and Bowen, A. J. (1995). Parametrization of orbital velocity asymmetries of shoaling and breaking waves using bispectral analysis. *Coastal Engineering*, *26*(1-2), 15–33.

Elfrink, B., Hanes, D. M., and Ruessink, B. G. (2006). Parameterisation and simulation of near bed orbital velocities under irregular waves in shallow water. *Coastal Engineering*, *53*(11), 915-927.

Elgar, S., Gallagher, E. L., and Guza, R. T. (2001). Nearshore sandbar migration. *Journal of Geophysical Research. C. Oceans*, *106*, 11623-11627.

Elgar, S. (1987). Relationships involving third moments and bispectra of a harmonic process. *IEEE transactions on acoustics, speech, and signal processing*, *35*(12), 1725-1726.

Fernandez-Mora A., (2015). On cross-shore beach profile morphodynamics. *Universitat Politecnica de Caralunya.* PhD Thesis.

Guza, R. T., and Thornton, E. B. (1980). Local and shoaled comparisons of sea surface elevations, pressures, and velocities. *Journal of Geophysical Research: Oceans*, *85*(C3), 1524-1530.

Isobe, M., and Horikawa, K. (1982). Study on water particle velocities of shoaling and breaking waves. *Coastal Engineering in Japan*, *25*, 109-123.

Jacobsen, N. G., Fuhrman, D. R., and Fredsøe, J. (2012). A wave generation toolbox for the open-source CFD library: OpenFoam®. *International Journal for Numerical Methods in Fluids*, *70*(9), 1073-1088.

Kennedy, A. B., Chen, Q., Kirby, J. T., and Dalrymple, R. A. (2000). Boussinesq modeling of wave transformation, breaking, and runup. I: 1D. *Journal of waterway, port, coastal, and ocean engineering*, *126*(1), 39-47.

Kim, J., Moin, P., and Moser, R. (1987). Turbulence statistics in fully developed channel flow at low Reynolds number. *Journal of fluid mechanics*, *177*, 133-166.

Malarkey, J., and Davies, A. G. (2012). Free-stream velocity descriptions under waves with skewness and asymmetry. *Coastal Engineering*, *68*, 78-95.

Manual, S. P. (1984). Department of the Army, Waterways Experiment Station, Corps of Engineers. *Coastal engineering researcher center*, *2*.

Ruessink, B. G., Michallet, H., Abreu, T., Sancho, F., Van der Werf, J. J., and Silva, P. A. (2011). Observations of velocities, sand concentrations, and fluxes under velocity-asymmetric oscillatory flows. *Journal of Geophysical Research: Oceans*, *116*(C3).

Ruessink, B. G., Ramaekers, G., and Van Rijn, L. C. (2012). On the parameterisation of the free-stream non-linear wave orbital motion in nearshore morphodynamic models. *Coastal Engineering*, *65*, 56-63.

Svendsen, I. A. (1984). Wave heights and set-up in a surf zone. *Coastal Engineering*, *8*(4), 303-329.

Svendsen, I. A. (1987). Analysis of surf zone turbulence. *Journal of Geophysical Research: Oceans*, *92*(C5), 5115-5124.

Van der A.D., van der Zanden J., O'Donoghue, T., Hunter D., Cáceres, I., McLelland, J.S., and Ribberink, J. S. (to be submitted). Hydrodynamics and turbulence under a large-scale plunging wave over a fixed bar.

Van den Broek. (2015). Water Particle Velocities under Shoaling and Breaking Waves. *University of Twente.* Bsc. Thesis.

Van der Zanden, J., Van der A, D. A., Hurther, D., Cáceres, I., O'Donoghue, T., and Ribberink, J. S. (2016). Near-bed hydrodynamics and turbulence below a large-scale plunging breaking wave over a mobile barred bed profile.Journal of Geophysical Research: Oceans.

List of symbols

The following are main symbols presented in this thesis. Other symbols are also used and defined in the text.

u_0 : Horizontal near-bed orbital velocity, m/s

U_w : Amplitude of near-bed orbital velocity, m/s

Sku : Skewness of horizontal near-bed orbital velocity, dimensionless

Asu : Asymmetry of horizontal near-bed orbital velocity, dimensionless

U_r : Ursell number, dimensionless

T : Wave period, s

ω : Angular frequency of wave, dimensionless

H : Wave height, m

L : Wavelength, m

h : Water depth, m

η : Surface elevation, m

ρ : Density of sea water, kg/m^3

g : Gravitational acceleration, m/s^2

ξ : Surf similarity, dimensionless

k_0^H : Depth-averaged turbulence from bed to the lower surface elevation profile, m^2/s^2

k_0 : Near-bed turbulence, m^2/s^2

ν : Eddy viscosity, m^2/s

E_w : Total wave energy, J/m^2

D_w : Total wave energy dissipation, J/m^2/s

D_r : Roller dissipation, J/m^2/s

D_f : Dissipation due to friction, J/m^2/s

List of Figures

class-mean values based on binning the individual estimates according to log(Ur) ±0.05. The vertical lines represent ± one standard deviation in each bin. The red dots are the data of Doering and Bowen (1995)."

Figure 4.6 Comparisons model results of H08T4 and field data regarding near-bed skewness (*Sku*) and asymmetry (*Asu*) as functions of the Ursell number (U_r). According to Ruessink *et al.* (2012), the grey dots are the individual estimates, in the filled ciecles are class-mean values based on binning the individual estimates according to log(Ur) ±0.05. The vertical lines represent ± one standard deviation in each bin. The red dots are the data of Doering and Bowen (1995)."

Figure 4.7 Near-bed orbital velocity skewness (*Sku*) and asymmetry (*Asu*) as functions of surf similarity (ξ) of cases H05T4 and H08T4. Panel A, C, E, and G are the dependencies in shoaling and breaking zones of corresponding cases. Panel B, D, F, and H are the dependencies in inner surf zone of corresponding cases. The dark lines are the fittings, with coefficient of determination R^2.

Figure 4.8 Near-bed orbital velocity skewness (*Sku*) and asymmetry (*Asu*) as functions of dimensionless wave energy dissipation ($D_w\ (U_w^3\rho)^{-1}$) of cases H05T4 and H08T4. The dark curves/lines are the fittings, with coefficient of determination R^2.

Figure 4.9 Near-bed orbital velocity skewness (*Sku*) and asymmetry (*Asu*) as functions of dimensionless roller dissipation ($D_r\ (U_w^3\rho)^{-1}$) of cases H05T4 and H08T4. Panel A, C, E, and G are the dependencies in shoaling and breaking zones of corresponding cases. Panel B, D, F, and H are the dependencies in inner surf zone of corresponding cases. The dark curves/lines are the fittings, with coefficient of determination R^2.

Figure 4.10 Near-bed orbital velocity skewness (*Sku*) and asymmetry (*Asu*) as functions of dimensionless dissipation due to bed friction ($D_f\ (U_w^3\rho)^{-1}$) of cases H05T4 and H08T4. Panel A, C, E, and G are the dependencies in shoaling and breaking zones of corresponding cases. Panel B, D, F, and H are the dependencies in inner surf zone of corresponding cases. The dark lines are the fittings, with coefficient of determination R^2.

Figure 4.11 Near-bed orbital velocity skewness (*Sku*) and asymmetry (*Asu*) as functions of dimensionless time-averaged near-bed turbulence ($<k_0>\ (gh)^{-1}$) of cases H05T4 and H08T4. Panel A, C, E, and G are the dependencies in shoaling and breaking zones of corresponding cases. Panel B, D, F, and H are the dependencies in inner surf zone of corresponding cases. The dark curves/lines are the fittings, with coefficient of determination R^2.

Figure 5.1 Dimensionless wave height (*H/h*) and dimensionless wave length (*L/h*) as functions of dimensionless roller dissipation ($D_r\ (U_w^3\rho)^{-1}$) of cases H05T4 and H08T4 respecticely.The dark curves are the fittings, with coefficient of determination R^2.

List of Tables

Appendix A

Depth-averaged turbulence

This appendix mainly show the depth-averaged turbulence as auxiliary tool to determine study area (from shoaling zone to inner surf zone), and hydrodynamics equilibrium for all cases respectively.

A.2.1 H05T4-SL15

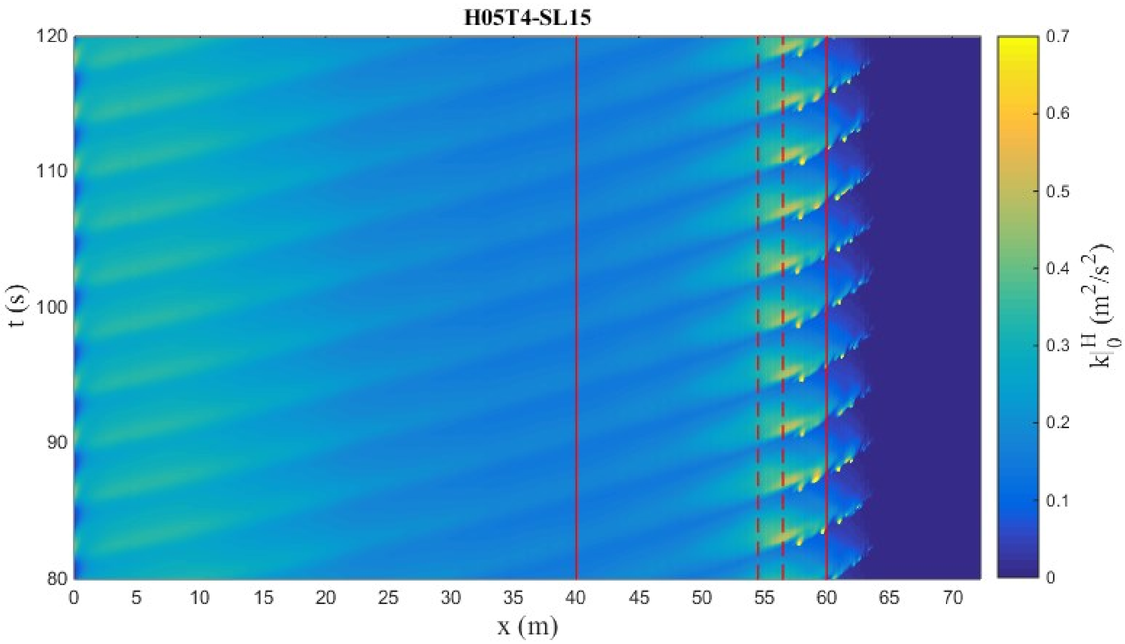

Figure A1 Contour map of depth-averaged turbulence in cross-shore domain after 80s runtime for H05T4-SL15. The study area is between red solid lines. The breaking zone is between red dashed lines.

The dimensionless depth-averaged turbulence of H05T4-SL15 is analysed for hydrodynamics equilibrium in Section 4.1.

A.2.2 H05T4-SL20

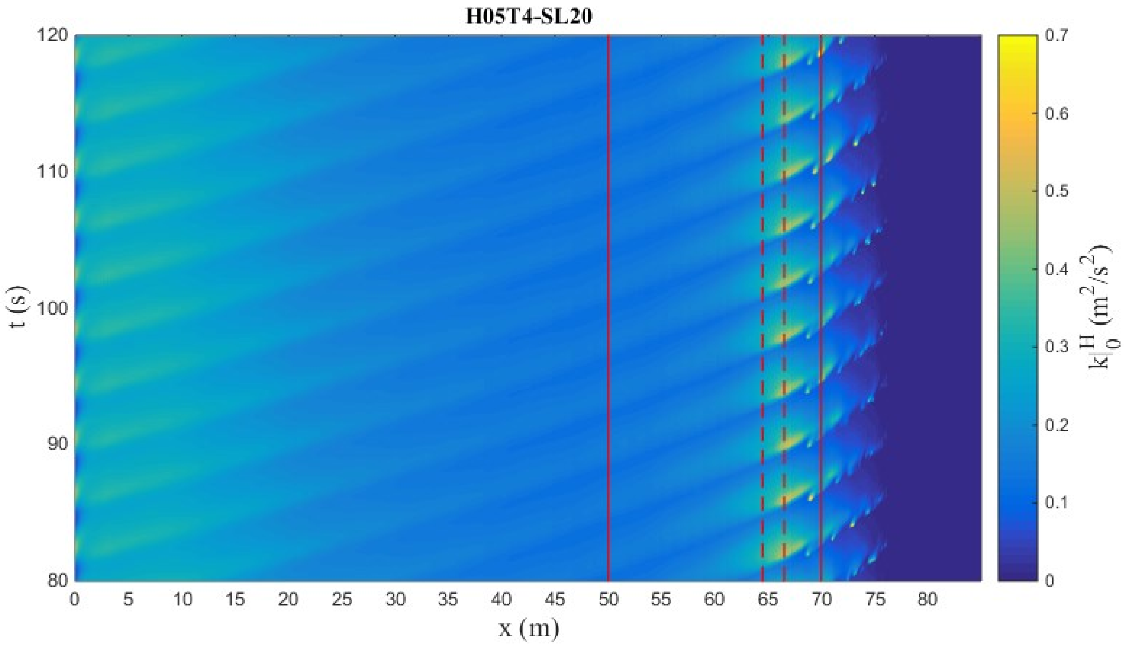

Figure A2 Contour map of depth-averaged turbulence in cross-shore domain after 80s runtime for H05T4 – SL20. The study area is between red solid lines. The breaking zone is between red dashed lines.

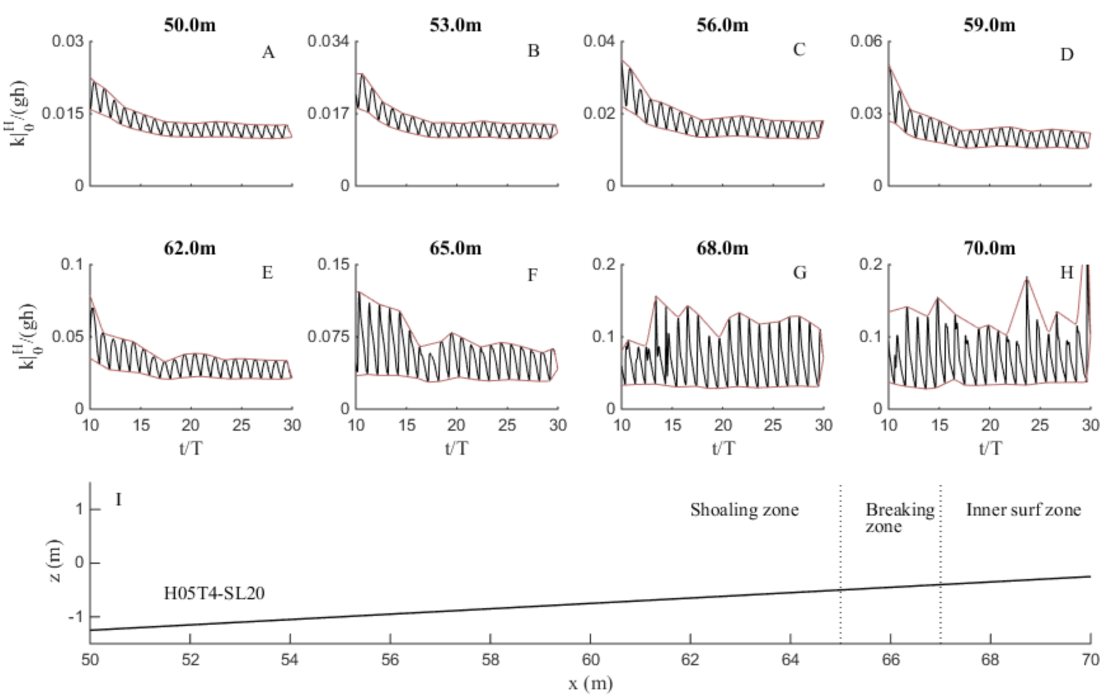

Figure A3 Dimensionless depth-averaged turbulence of H05T4 as function of time. Panel A to H are cross-shore locations with 3.0m interval in study area of SL20. In panel I, the thick dark line is the bed profile; the dotted dark lines partition the study region as shoaling zone, breaking zone, and inner surf zone.

A.2.3 H05T4-SL25

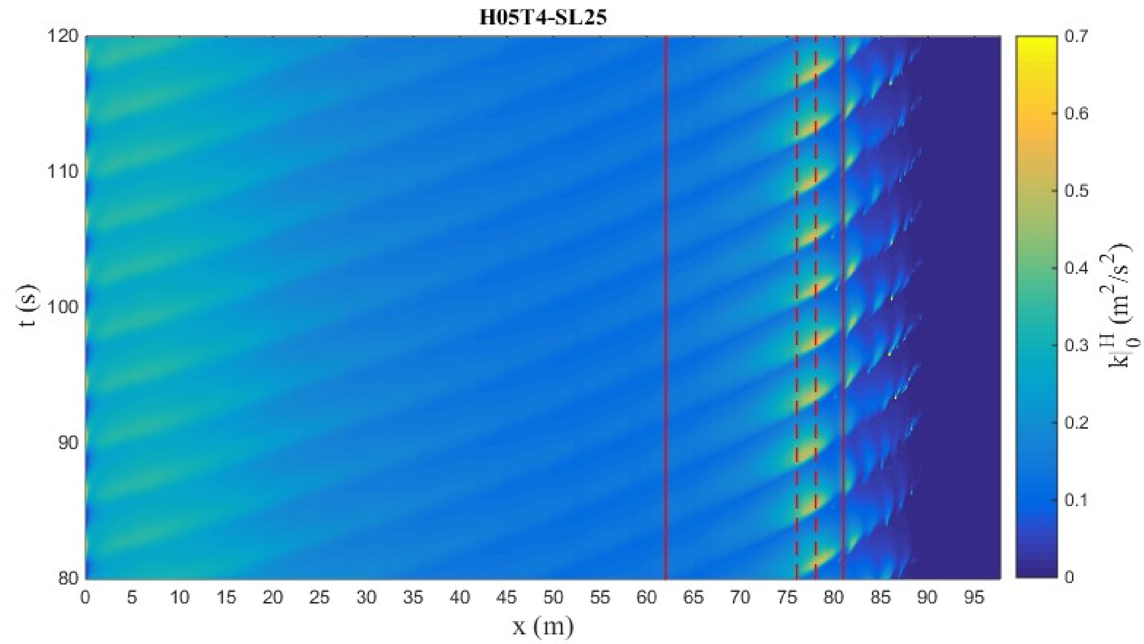

Figure A4 Contour map of depth-averaged turbulence in cross-shore domain after 80s runtime for H05T4-SL25. The study area is between red solid lines. The breaking zone is between red dashed lines.

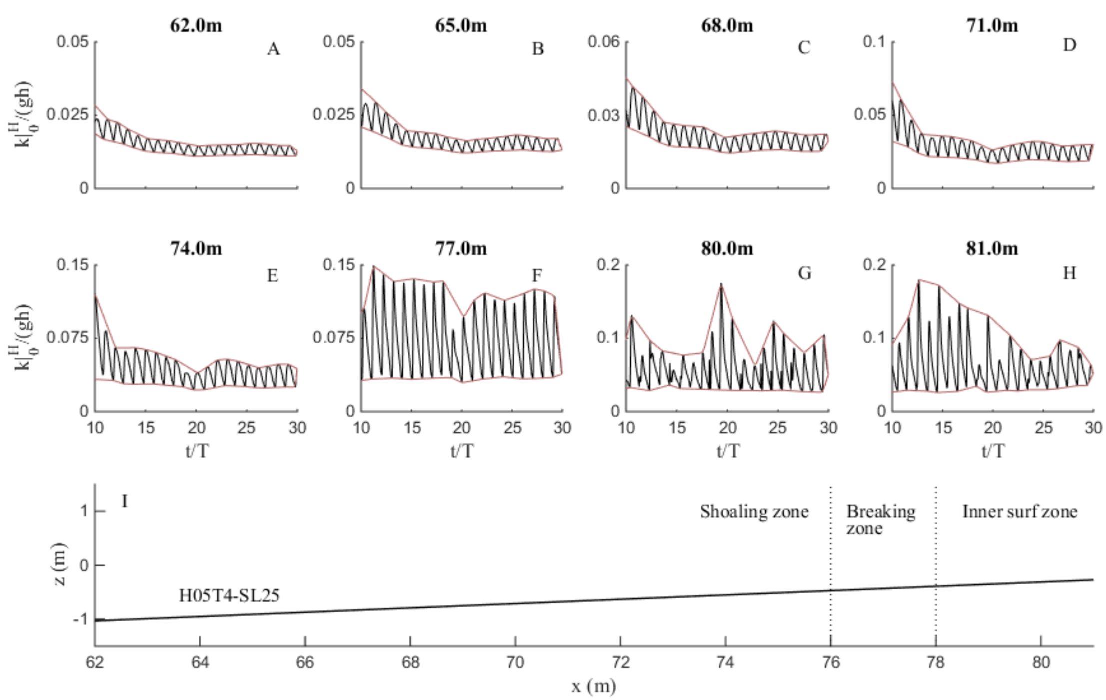

Figure A5 Dimensionless depth-averaged turbulence of H05T4 as function of time. Panel A to H are cross-shore locations with 3.0m interval in study area of SL25. In panel I, the thick dark line is the bed profile; the dotted dark lines partition the study region as shoaling zone, breaking zone, and inner surf zone.

A.2.4 H08T4-SL15

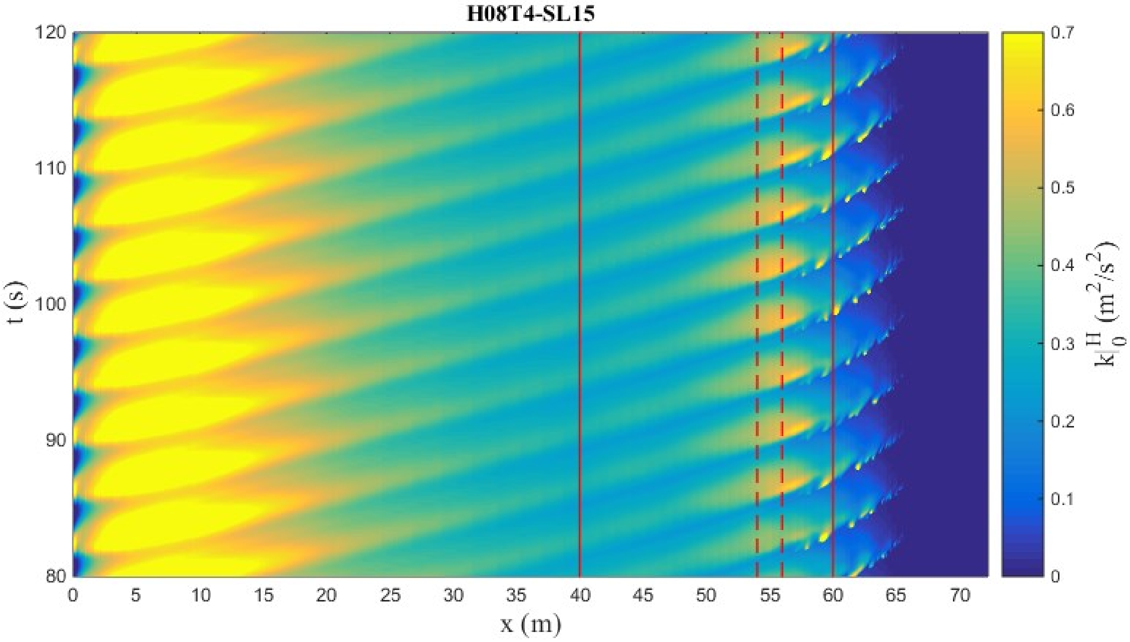

Figure A6 Contour map of depth-averaged turbulence in cross-shore domain after 80s runtime for H08T4 – SL15. The study area is between red solid lines. The breaking zone is between red dashed lines.

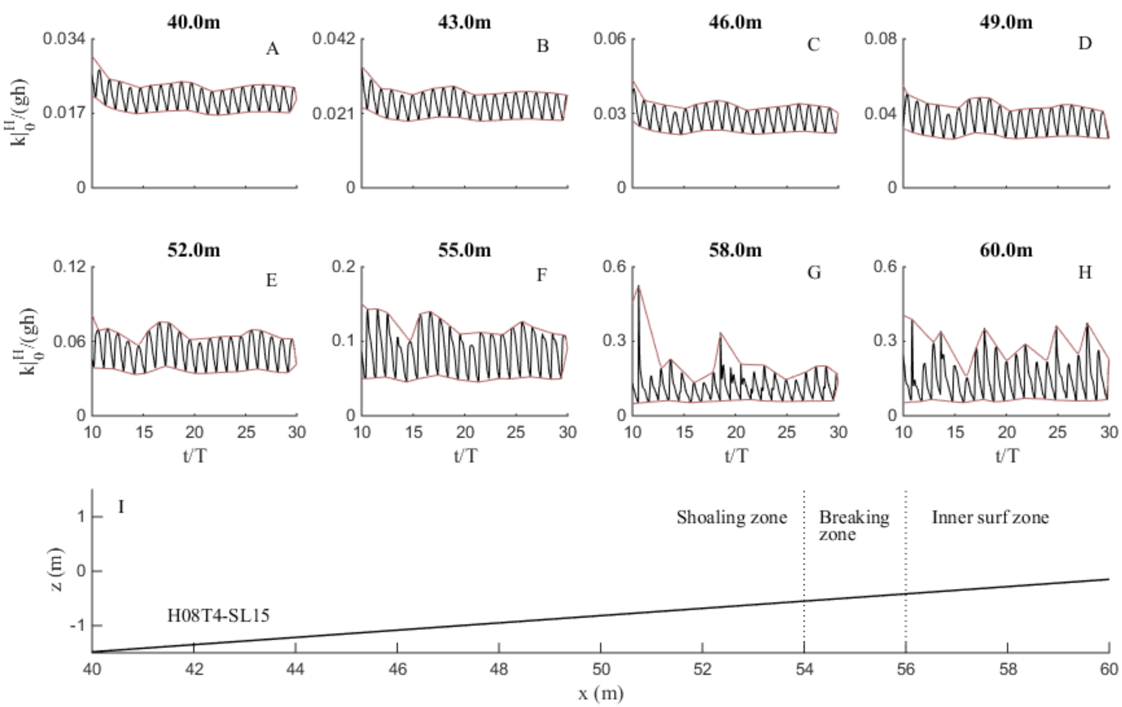

Figure A7 Dimensionless depth-averaged turbulence of H08T4 as function of time. Panel A to H are cross-shore locations with 3.0m interval in study area of SL15. In panel I, the thick dark line is the bed profile; the dotted dark lines partition the study region as shoaling zone, breaking zone, and inner surf zone.

A.2.4 H08T4-SL20

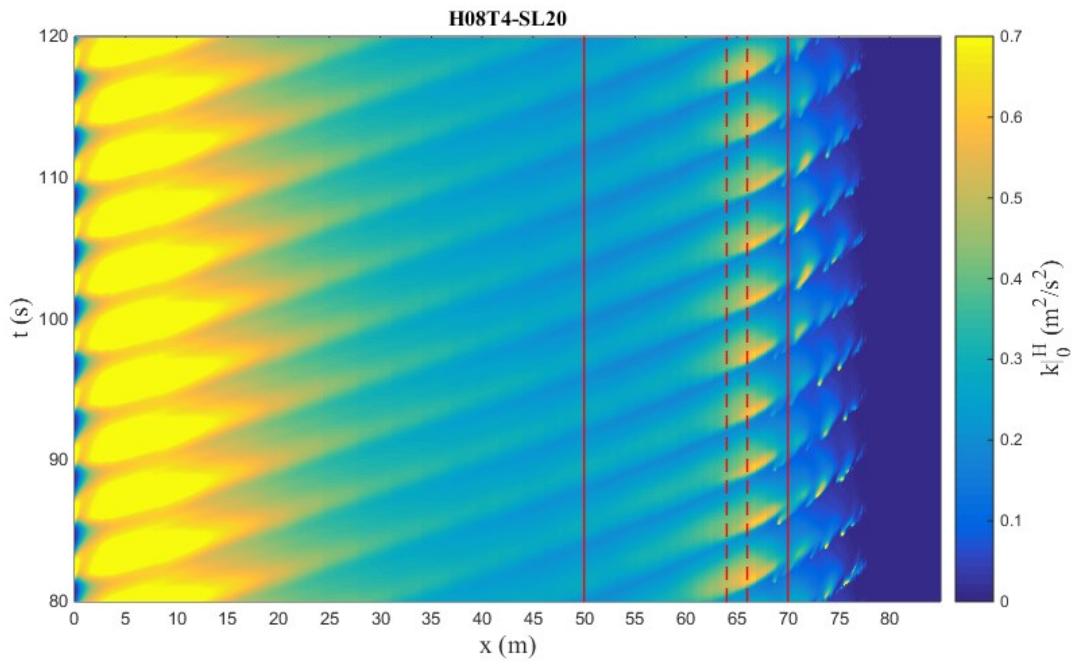

Figure A8 Contour map of depth-averaged turbulence in cross-shore domain after 80s runtime for H08T4-SL20. The study area is between red solid lines. The breaking zone is between red dashed lines.

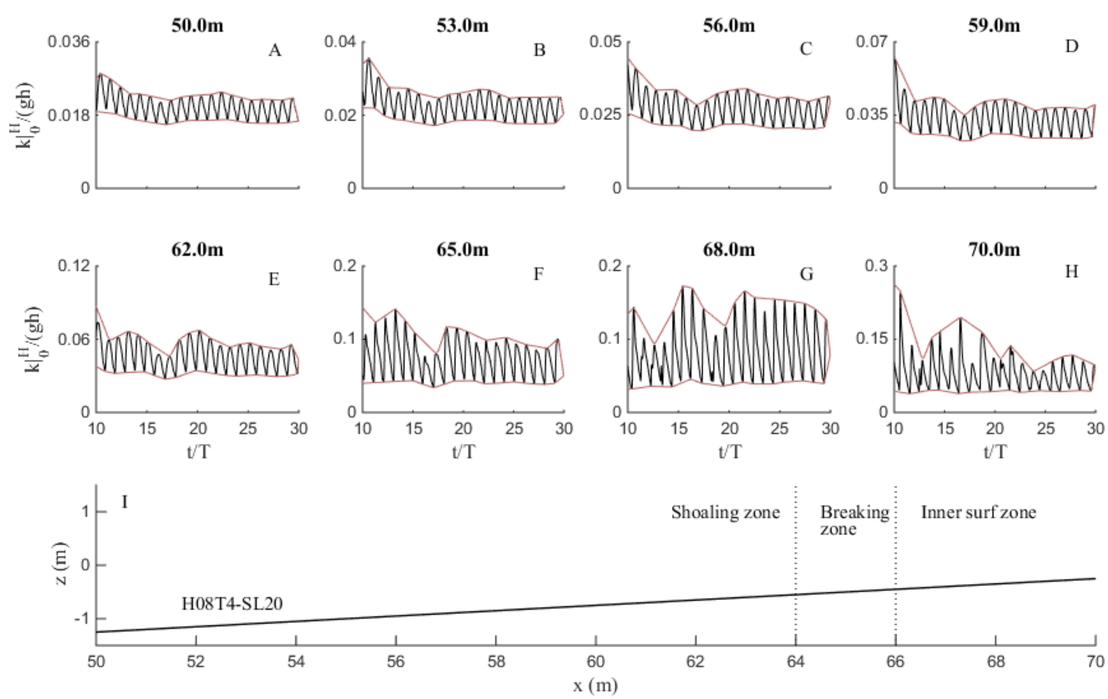

Figure A9 Dimensionless depth-averaged turbulence of H08T4 as function of time. Panel A to H are cross-shore locations with 3.0m interval in study area of SL20. In panel I, the thick dark line is the bed profile; the dotted dark lines partition the study region as shoaling zone, breaking zone, and inner surf zone.

A.2.4 H08T4-SL25

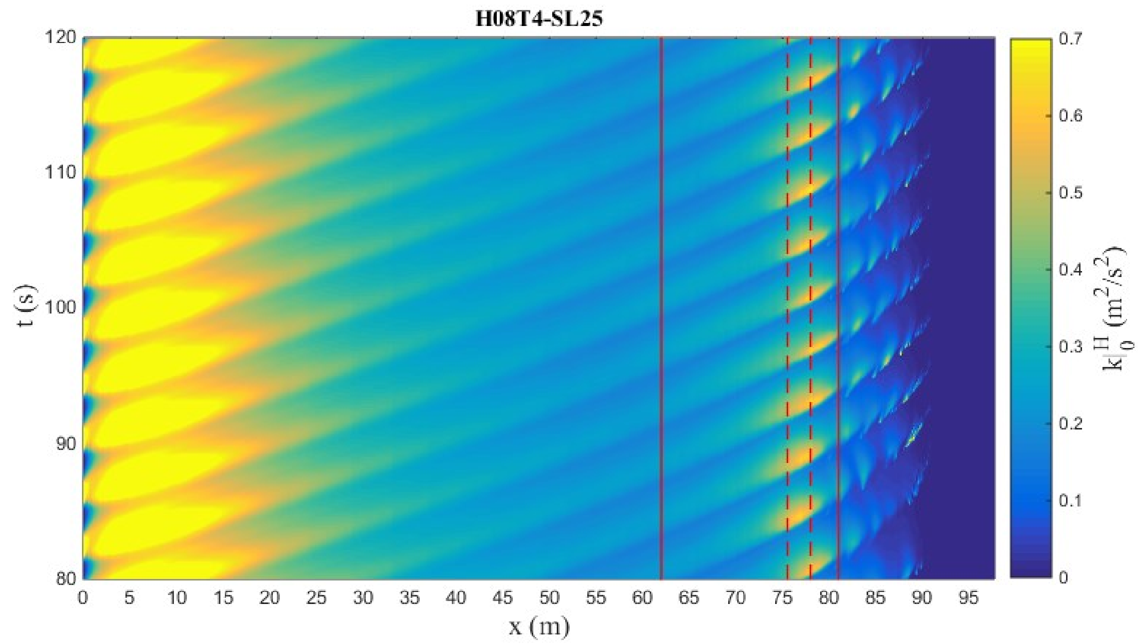

Figure A10 Contour map of depth-averaged turbulence in cross-shore domain after 80s runtime for H08T4-SL25. The study area is between red solid lines. The breaking zone is between red dashed lines.

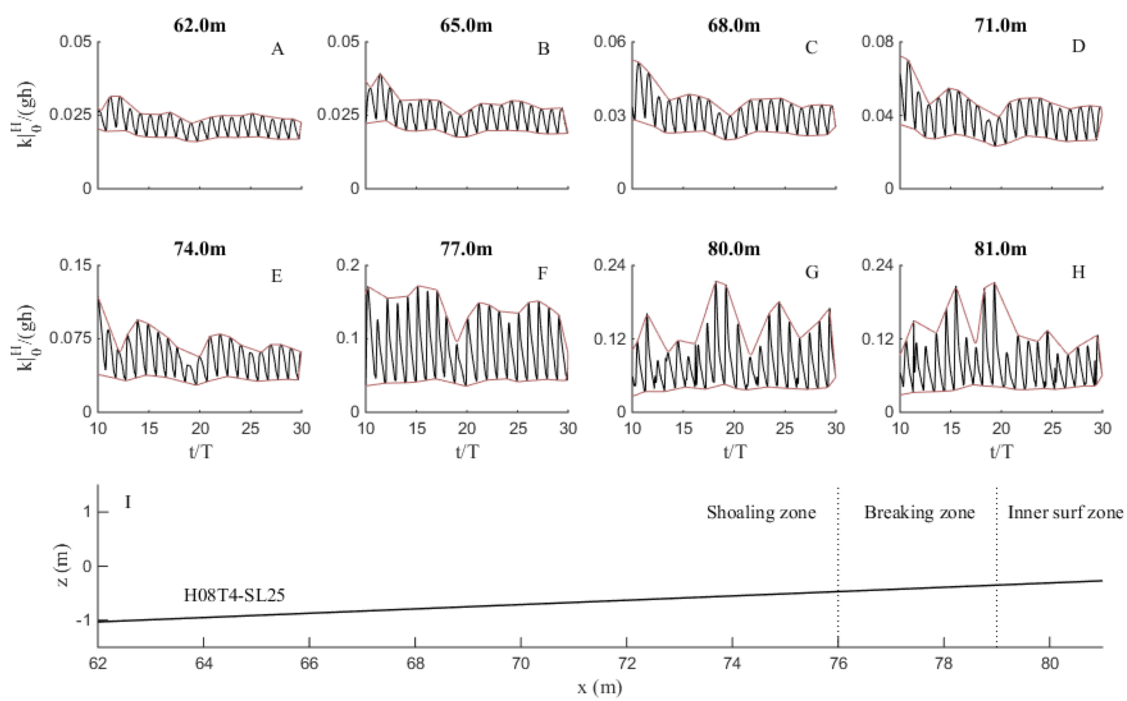

Figure A11 Dimensionless depth-averaged turbulence of H08T4 as function of time. Panel A to H are cross-shore locations with 3.0m interval in study area of SL25. In panel I, the thick dark line is the bed profile; the dotted dark lines partition the study region as shoaling zone, breaking zone, and inner surf zone.

Appendix B

Data extraction and treatment

To facilitate model validation and dependencies study, in this appendix, Section B.1 introduces the method to select required model data from computational cells. And, Section B.2 explains the critical data treatment for further analysis, in terms data averaging, mean value removal, and computing turbulence.

B.1 Data extraction

In the model validation, surface elevation, horizontal oscillatory velocity, and turbulence are used. The horizontal velocity data was selected at the corresponding locations of ADVs (10cm, 40cm, and 80cm above the bed). Note that waves2Foam outputs water-air interface coefficient α to represent free surface instead of the surface elevation itself. Therefore, a tracking process. According to Jacobsen *et al.*, 2012, α is 1 when a computational cell is filled with water and is 0 when the cell is empty but air. The critical value of α is decided to be 0.8, i.e. the computational grids which has α greater than 0.8 is considered to be a part of water surface. Although the use of constant α could result in unsmoothed water surface (see Figure B.1), this is a resolved choice which ensures the water surface is tracked as accurate as possible from shoaling zone to inner surf zone for all cases.

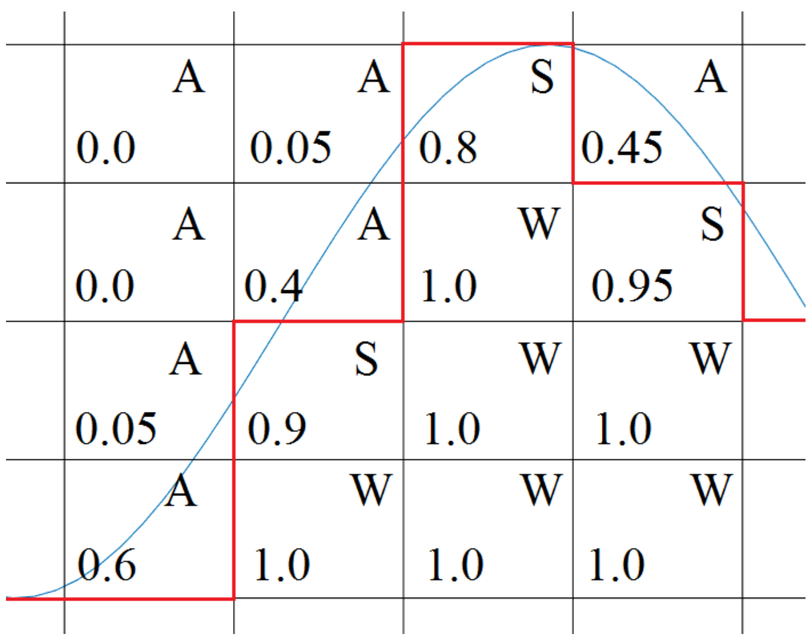

Figure B.1 An overview of the method of determining water surface by water-air interface (α). Blue curve is the sinusoidal water surface; Red line is the water surface determined by α=0.8. "A", "S", and "W" mean the computational is defined as air, water surface, and water body respectively. Note that in computational cells, α values given by roughly estimation.

B.2 Data treatment

B.2.1 Averaging

The experimental data of surface elevation, and near-bed velocity were already phase-averaged, thus averaging is done for experimental turbulence (computed in Section B.2.3), and model data. In this research, data is averaged by phase, time, and depth for different usages. For arbitrary time-dependent variable Φ(t) is phase-averaged as

$$<\Phi(t)>=\frac{1}{N}\sum_{n=1}^{N}\Phi(t+(n-1)T) \tag{B.1}$$

where N is the amount of wave cycles, T is the wave period. N is 4 for SINBAD simulation and is 10 for case studies, according hydrodynamics equilibrium respectively. Bases on Eqn. (B.1), the time-averaged variable is

$$\bar{\Phi}=\frac{1}{T}\int_{0}^{T}<\Phi(t)>dt \tag{B.2}$$

Then, only simulated turbulence, and eddy viscosity for case studies are depth and time-averaged arbitrary variable is calculated as

$$\hat{\Phi}=\frac{1}{h}\int_{0}^{H_{low}}<\Phi(t)>dh \tag{B.3}$$

where h is the local water depth, H_{low} is the low envelope of surface elevation. Choosing low envelope of surface elevation is under the consideration that the model validation regarding turbulence is done from bottom to upper ADVs (average ~0.3m lower than SWL). And the validation results show that simulated turbulence is less reliable at higher water column due to overestimation.

B.2.2 Near-bed orbital velocity

The phase-averaged near-bed orbital velocity is required for computing skewness (Eqn. 1) and asymmetry (Eqn. 2). However, horizontal near-bed velocity from both ADVs and model simulations consists of oscillatory velocity and mean flow. The mean flow is removed from orbital velocity as

$$u_0(t)=u(t)-\bar{u}(t) \tag{B.4}$$

here $u(t)$ is near-bed velocity, and $\bar{u}(t)$ is the mean current.

B.2.3 Experimental turbulence

Turbulence is one of the outputs from model simulation. For experimental data, ADVs measured turbulence components. According to Svendsen (1987), the experimental turbulence can be calculated by

$$k(t) = \frac{1}{2}[u'(t)^2 + v'(t)^2 + w'(t)^2] \tag{B.5}$$

where *u'(t)*, *v'(t)*, and *w'(t)* are the turbulence components of velocity in horizontal, lateral, and vertical direction respectively.

Appendix C
Ruessink-Abreu parameterisation

Ruessink *et al.* (2012) proposed parameterisation regarding near-bed orbital velocity skewness and asymmetry to predict near-bed orbital velocity, by incorporating with the expression of free-stream velocity presented by Abreu *et al*. (2010):

$$u_0(t) = U_w f \frac{\sin \omega t + r \sin \phi / (1+f)}{1 - r \cos(\omega t + \phi)} \tag{C.1}$$

where t is the time; U_w is the amplitude the near-bed orbital velocity computed by linear wave theory (Eqn. 2.8); $\omega = 2\pi/T$ is the angular frequency, ϕ is a phase, r is a non-linearity measure, and $f = \sqrt{1-r^2}$ is a dimensionless factor that ensures that the amplitude of u_0 is equal to U_w.

To solve r and ϕ, Ruessink *et al.* (2012) used the Eqns. from (C.2) to (C.5).

The total non-linearity B and the phase ψ depend on the Ursell number Ur (Eqn. 2.2) as

$$B = p_1 + \frac{p_2 - p_1}{1 + \exp[(p_3 - \log U_r)/p_4]} \tag{C.2}$$

$$\psi = -90° + 90° \tanh(p_5 / U_r^{p_6}) \tag{C.3}$$

where p_1=0, p_2=0.857, p_3=-0.471, p_4=0.297, p_5=0.815, and p_6=0.672 considering the 95% confidence interval.

Parameters r and ϕ relate to B and ψ as

$$B = 3b / \sqrt{2(1-b^2)} \tag{C.4}$$

with $b = r / (1 + \sqrt{1-r^2})$, and

$$\phi = -\psi - \pi / 2 \tag{C.5}$$

As the range of r is (0, 1), and ϕ is $(-\frac{\pi}{2}, 0)$ are given by Ruessink *et al.* 2012, in this research, r and ϕ are solved by iteration.